Sedimentary Geology 489 (2025) 106959

Contents lists available at ScienceDirect

Sedimentary Geology

journal homepage: www.elsevier.com/locate/sedgeo

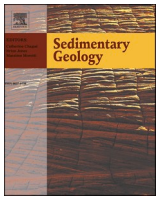

# Cambrian reef complexes and pelmatozoan-rhynchonelliformean meadows from the Alborz Mountains, northern Iran: A reassessment of the Miaolingian–Furongian paucity of metazoan reefs paradigm

J. Javier Álvaro [a,*], Aram Bayet-Goll [b], Mehdi Daraei [b], Blanca Martínez-Benítez [a]

[a] Institute of Geosciences (CSIC-UCM), Dr. Severo Ochoa 7, 28040, Madrid, Spain
[b] Institute for Advanced Studies in Basic Sciences (IASBS), Zanjan, Iran

ARTICLE INFO

Editor: Dr. Catherine Chagué

*Keywords:*
Carbonate
Reef
Hardground
Cambrian
Gondwana

ABSTRACT

The Alborz Mountains in northern Iran represent one of the few exceptions to the worldwide decline in Miaolingian–Furongian (Cambrian) carbonate abundance and reefal volume, likely related to the arrival of northeastern Gondwana to subtropical latitudes. This Gondwana margin recorded the stepwise nucleation of microbial and shelly carbonate factories, lithostratigraphically recognized as members of the Lalun and Mila formations. The late Cambrian Epoch 2 to Miaolingian interval displays the development of oncoid-pisoid accumulations and microbial build-ups, with laminated and clotted textures, in open-sea and protected (back-barrier) settings. In contrast, the late Miaolingian and Furongian interval recorded a generalized establishment of pelmatozoan-rhynchonelliformean meadows, locally affected by horst-and-graben topographies. Hanging-wall blocks offered some protection from high-energy, shallow-water conditions, which favoured the growth of anthaspidellid-microbial reef complexes. The primary porosity recorded in the pelmatozoan-rhynchonelliformean shell beds, and the associated microboring and micritization of skeletal walls, favoured the episodic development of carbonate and iron oxyhydroxide hardgrounds. Such a singularity leads to the development of a more comprehensive global model linked to Miaolingian–Furongian progressive declines in $^{87}Sr/^{86}Sr$ ratios, estimated extent of carbonate platforms and reefal volume and atmospheric $O_2$ (punctuated by a sharp increase related to the SPICE event), coeval with relative increases in seawater calcite saturation. In some subtropical areas, such as in the Alborz margin of Gondwana, the re-occurrence of metazoan frame-builders took place in late Miaolingian times, and their subsequent reefal success was primarily controlled by tectonic activity and the nucleation of hardgrounds in highly porous pelmatozoan-rhynchonelliformean shell beds.

## 1. Introduction

The decline and virtual extinction of archaeocyaths across the Cambrian Epoch 2–Miaolingian (former 'lower–middle Cambrian') boundary interval were recognized as a global extinction crisis in the early 1990s (e.g., Debrenne, 1991; Signor, 1992). Putative archaeocyaths were subsequently reported from the Miaolingian Neptune Limestone (Wood et al., 1992) and the Furongian Minaret Formation (Debrenne et al., 1984; Debrenne and Kruse, 1989) from Antarctica, although the taxonomic affinity of the latter was subsequently reinterpreted as a potential anthaspidellid demosponge (Lee, 2024). The succeeding Miaolingian–Furongian interval was depleted on metazoan reefs, which did not particularly re-establish globally until Early Ordovician times, when spiculate demosponges and primitive bryozoans, corals receptaculitaleans and stromatoporoids contributed to reefal framework (e.g., Webby, 2002; Adachi et al., 2011; Hong et al., 2015, 2022; Li et al., 2015).

The apparent Miaolingian–Furongian scarcity in metazoan reefs coincided with a global persistent fall in the relative abundance of preserved carbonates and reefal volume, excluding purely microbial reefs, of three orders of magnitude, from about $10^7$ to $10^4$ $m^3$ (Riding and Liang, 2005; Smith et al., 2021; Raja et al., 2023). However, this kind of statistical databases has not yet considered basins where carbonate production and non-reefal and reefal volume increased throughout Miaolingian–Furongian times, as in the case study represented by the Alborz margin of northeastern Gondwana.

* Corresponding author.
*E-mail address:* jj.alvaro@csic.es (J.J. Álvaro).

https://doi.org/10.1016/j.sedgeo.2025.106959
Received 16 July 2025; Received in revised form 25 August 2025; Accepted 29 August 2025
Available online 3 September 2025
0037-0738/© 2025 The Authors. Published by Elsevier B.V. This is an open access article under the CC BY license (http://creativecommons.org/licenses/by/4.0/).

The aims of this paper are (i) to analyse and revise the sedimentary and palaeogeographic factors that controlled the nucleation, growth and demise of Cambrian Epoch 2 to Furongian microbial and microbial-shelly carbonate factories developed in the Alborz Basin; (ii) to interpret the microbial and early-diagenetic influence in the onset of firmgrounds and hardgrounds and the development of pelmatozoan-rhynchonelliformean meadows (the Rhynchonelliformea is a major subphylum and clade of brachiopods with hard calcium carbonate shells; Williams et al., 2002); (iii) to constrain the tectonic control on reefal vs. non-reefal growth; and (iv) to reassess the paradigm of the Miaolingian–Furongian paucity of metazoan reefs in this specific margin of Gondwana, which contradicts the coeval worldwide fall in carbonate production and reefal preservation.

## 2. Palaeogeographic and stratigraphic overview

The Cambrian counter-clockwise rotation of Gondwana controlled the poleward migration of its Moroccan-SW European margin, which led to the disappearance of their characteristic microbial-archaeocyathan carbonate factories across the Cambrian Epoch 2–Miaolingian transition (Scotese and Barret, 1990; Mitchell et al., 2010; Álvaro et al., 2013a, 2016). As long as this margin gradually left low-latitudes, the Alborz margin of northeastern Gondwana (Fig. 1A) arrived to subtropical latitudes and recorded the transition from Terreneuvian mixed (carbonate-siliciclastic) depositional systems to late Cambrian Epoch 2–Miaolingian microbial-dominant carbonate factories, and Furongian blanketing of pelmatozoan meadows locally punctuated by anthaspidellid-microbial patch reefs (Hamdi et al., 1995; Lasemi and Amin-Rasouli, 2007; Kruse and Zhuravlev, 2008; Popov et al., 2013; Bayet-Goll et al., 2015, 2021; Devaere et al., 2021; Spina et al., 2021; Sorci et al., 2023); the Anthaspidellidae is a family of lithistid sponges with dendrocline spicules formed by ladder-like trabs (Finks, 2003a, 2003b). The final demise of carbonate productivity was marked by generalized drowning steps, probably related to tectonic episodes associated with rifting conditions, and poisoning of carbonate factories by the influence of cool waters and siliciclastic input during the Early Ordovician (Álvaro et al., 2022; Ghobadi Pour et al., 2022; Bayet-Goll et al., 2023; Daraei et al., 2023). Six distinct episodes of carbonate production, including different frame-building textures and fabrics, can be recognized in the upper Cambrian Series 2 to Furongian strata of the eastern Alborz Mountains (Fig. 2). They are lithostratigraphically assigned to the Lalun Formation and the Mila Formation or Group.

The Lalun Formation consists of sandstones and subsidiary shale interbeds, interpreted as a mosaic of fluvial and tidally influenced estuarine environments (Bayet-Goll et al., 2018, 2021). The formation can reach 532 m in thickness, but pinches out northward and northwestward (Azerbaijan Province of Iran), where it unconformably overlies a Proterozoic basement (Stöcklin, 1972). Its age is based on the

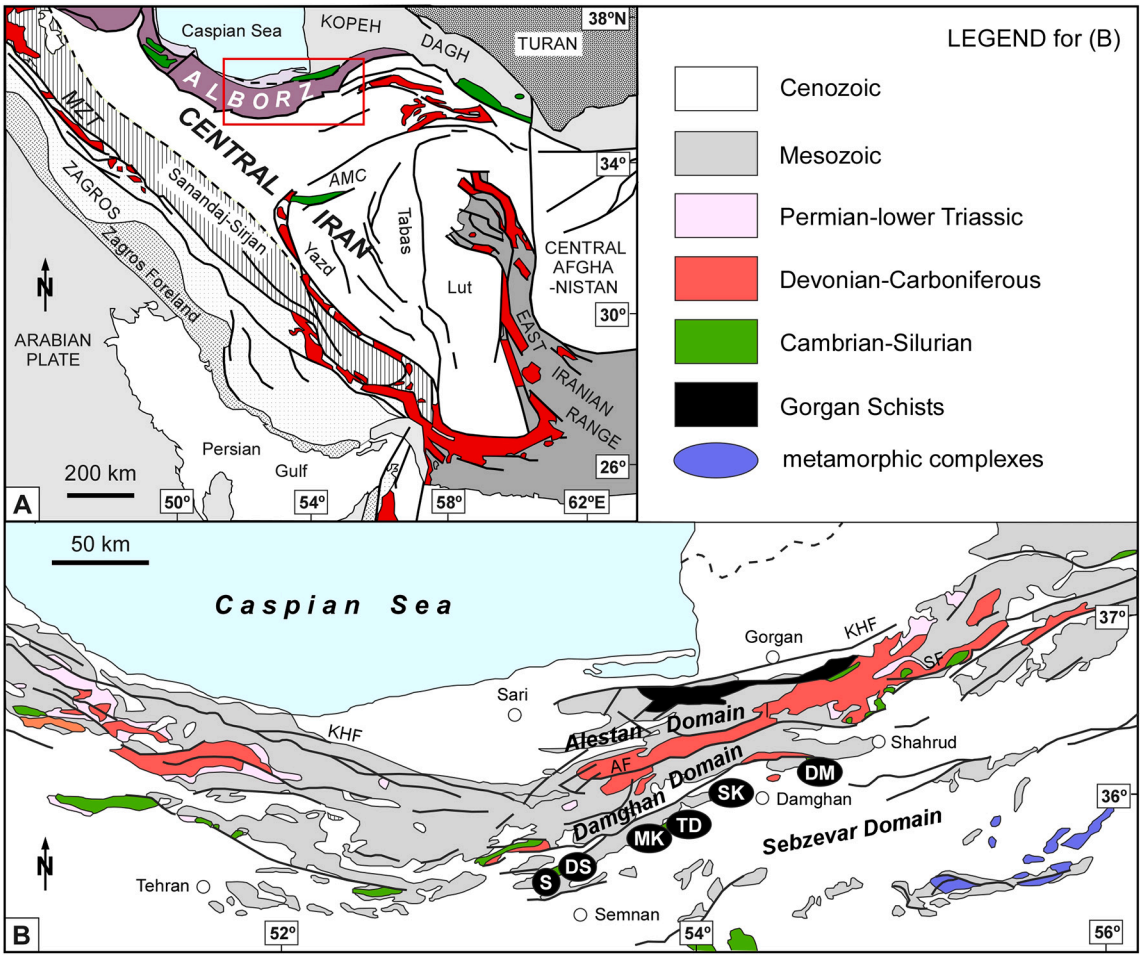


**Fig. 1.** A. Main tectonic units of Iran; Eocimmerian units are marked in green, Mesozoic ophiolites along the Main Zagros and other sutures in black, and Alborz Mountains in purple. B. Simplified geological map of the Alborz Ranges (boxed in A), northern Iran, with setting of stratigraphic sections mentioned in the text. Abbreviations: AF, Astaneh Fault; AMC, Anarak Metamorphic Complex; DM, Deh-Molla (GPS coordinates: N36°21'19.66", E54°45'01.90"); DS, Deh-Sufiyan (N35°47'36", E53°18'55"); MK, Mila-Kuh (N35°58'54", E53°48'45"); KHF, Khazar Thrust Fault; MZT, Main Zagros Thrust; S, Shahmirzad (35°47'29.07"N, 53°18'45.00"E); SF, Shahrud Fault; SK, Simeh-Kuh (36°12′42.9″N, 54°13′36.1″E); and TD, Tuyeh-Darvar (N36°26'54.67", E54°10'36.87").
Modified from Álvaro et al. (2022).

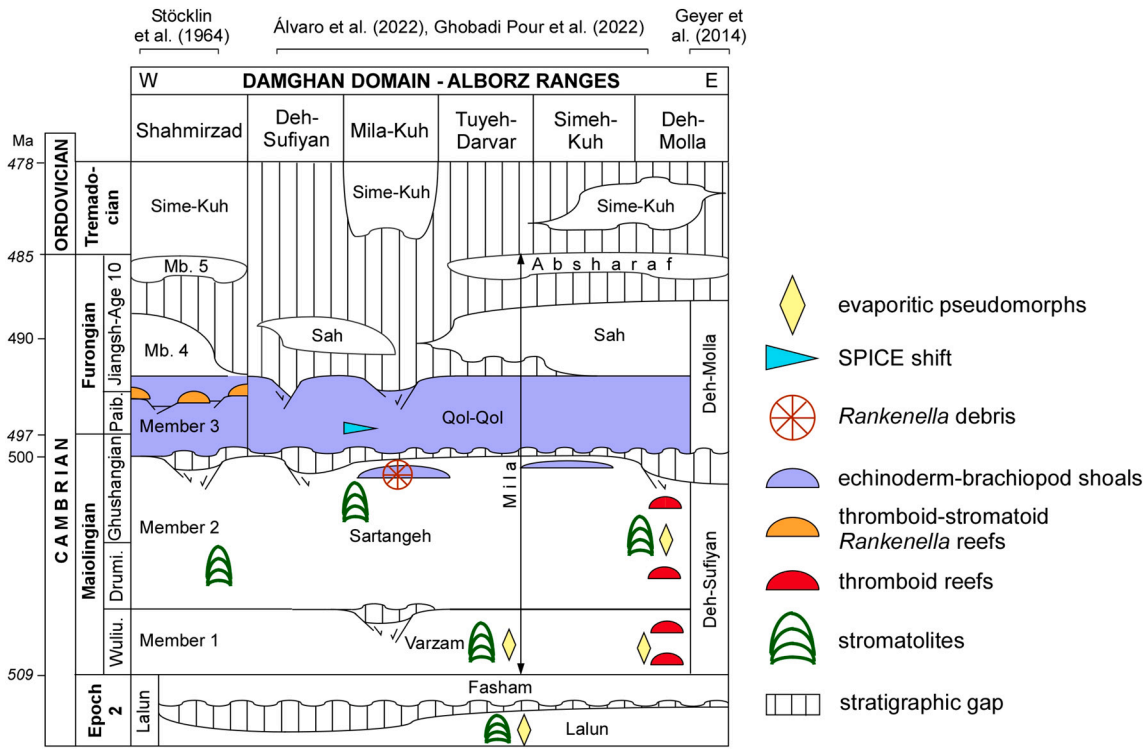


**Fig. 2.** Updated Cambrian Series 2–Tremadocian stratigraphic chart of the eastern Alborz Ranges showing setting of major unconformities, gaps and location of the main reef complexes reported in the text. Abbreviations: Drumi., Drumian; Jiangsh., Jiangshanian; Paib., Paibian; Wuliu., Wuliuan. Modified after Geyer et al. (2014) and Álvaro et al. (2022).

presence of *Cruziana* and *Rusophycus* ichnospecies (Ruttner et al., 1968; Hamdi, 1995; Seilacher, 2007; Bayet-Goll et al., 2018). The most chronostratigraphically significant ones, *C. cantabrica* and *C. nabataeica*, would suggest a broad Cambrian Epoch 2 time (Buatois and Mángano, 2011). An upper informal member, up to 35 m thick, has been reported in the eastern Alborz Ranges composed of variegated (reddish, purple and green) shales interbedded with sandstones and stromatolitic carbonates. At the Tuyeh-Darvar section (Figs. 2–3), Lasemi and Amin-Rasouli (2007) reported the presence of archaeocyaths, but such assertion was subsequently discarded by Kruse and Zhuravlev (2008) and Geyer et al. (2014). This outcrop is revisited below.

The Fasham Formation (former 'Top Quartzite'; Hamdi, 1995) unconformably overlies the Lalun Formation, and comprises amalgamated sandstone sets and conglomerate channels interpreted as tidal shoal complexes infilling an inherited palaeorelief (Bayet-Goll et al., 2018, 2021). The basal incision of the Fasham Formation (Fig. 2) has been traditionally linked to a global eustatic fall, known as the Hawke Bay, Toyonian or Daroca Regression (Palmer and James, 1980; Álvaro and Vennin, 1998; Nielsen and Schovsbo, 2015; Lasemi and Amin-Rasouli, 2016).

The conformably overlying Mila Formation *sensu* Stöcklin et al. (1964) is a heterolithic succession of dolostone, limestone, marlstone and shale (Fig. 3), grading in its uppermost part into sandstone/shale alternations. Originally, the formation was subdivided into five members, although the original definition of its fifth member was somewhat ambiguous (for a recent revision, see Álvaro et al., 2022). The three lower members, dominated by carbonate strata, were numbered 1 to 3 by Stöcklin et al. (1964). Geyer et al. (2014) modified the concept of the Mila Formation, subdividing the Mila Group into the Fasham, Deh-Sufiyan (former members 1 and 2) and Deh-Molla (member 3 and 4) formations, but its upper stratigraphic part was still unresolved. Finally, Álvaro et al. (2022) named Varzam, Sartangeh and Qol-Qol members to Members 1 to 3 *sensu* Stöcklin et al. (1964), on which this work is focused. The stratigraphic correlation of these lithostratigraphic frameworks is illustrated in Fig. 2. For the sake of simplicity, the three lower members of the Mila Formation defined by Stöcklin et al. (1964) will be followed.

Member 1 of the Mila Formation is 100–190 m thick and consists of brownish to grey carbonates with chert bands and variegated marlstone/shale interbeds. Regardless of widespread dolomitization, some limestone interbeds can be recognized. Despite the local presence of disarticulated trilobite sclerites, no biostratigraphically significant fossils have been so far reported.

Member 2, ca. 90 m thick, is composed of marly and sandy grey limestones alternating with green shales. In the vicinity of Shahmirzad town, a ribbon unit, characterized by millimetre- to centimetre-scale carbonate beds interlayered with carbonate conglomerates, has been interpreted as remains of episodically burrowed substrates developed in a wave- to storm-dominated environment (Bayet-Goll et al., 2015; Abbassi and Hadi, 2023). Also at Shahmirzad, the member has been subdivided into two Miaolingian, trilobite-based biostratigraphic units, named *Iranoleesia* and *Chelidonocephalus* zones (Kushan, 1973, 1978; Wittke, 1984; Peng et al., 1999), which display some distinct rhynchonelliform brachiopod shell beds rich in *Diraphora*? and *Nisusia* (Holmer et al., 2019).

The base of Member 3 is marked by a distinct unconformity, which locally preserves up to 8 m of erosive incision (e.g., Deh-Mola section; Álvaro et al., 2022: figs. 7g, 8a). In some areas (e.g., Mila-Kuh stratotype, Shahmirzad and Deh-Sufian logs), both the base and significant parts of the member are affected by synsedimentary listric normal faults subsequently sealed by overlying strata (Álvaro et al., 2022: figs. 7h, 8b–d). The member, ca. 80 m thick, consists of white to pinkish, partly glauconitic, thin- to medium-bedded limestones, dominated by alternations of echinoderm-brachiopod packstones and grainstones, and subsidiary shales. At Shahmirzad, the member has been subdivided, from bottom to top, into the Furongian, trilobite-based *Palaedotes–Torifera* and *Prochuangia* zones (Peng et al., 1999; Geyer et al., 2014). Some rhynchonelliform brachiopods (billingsellids *Billingsella*?

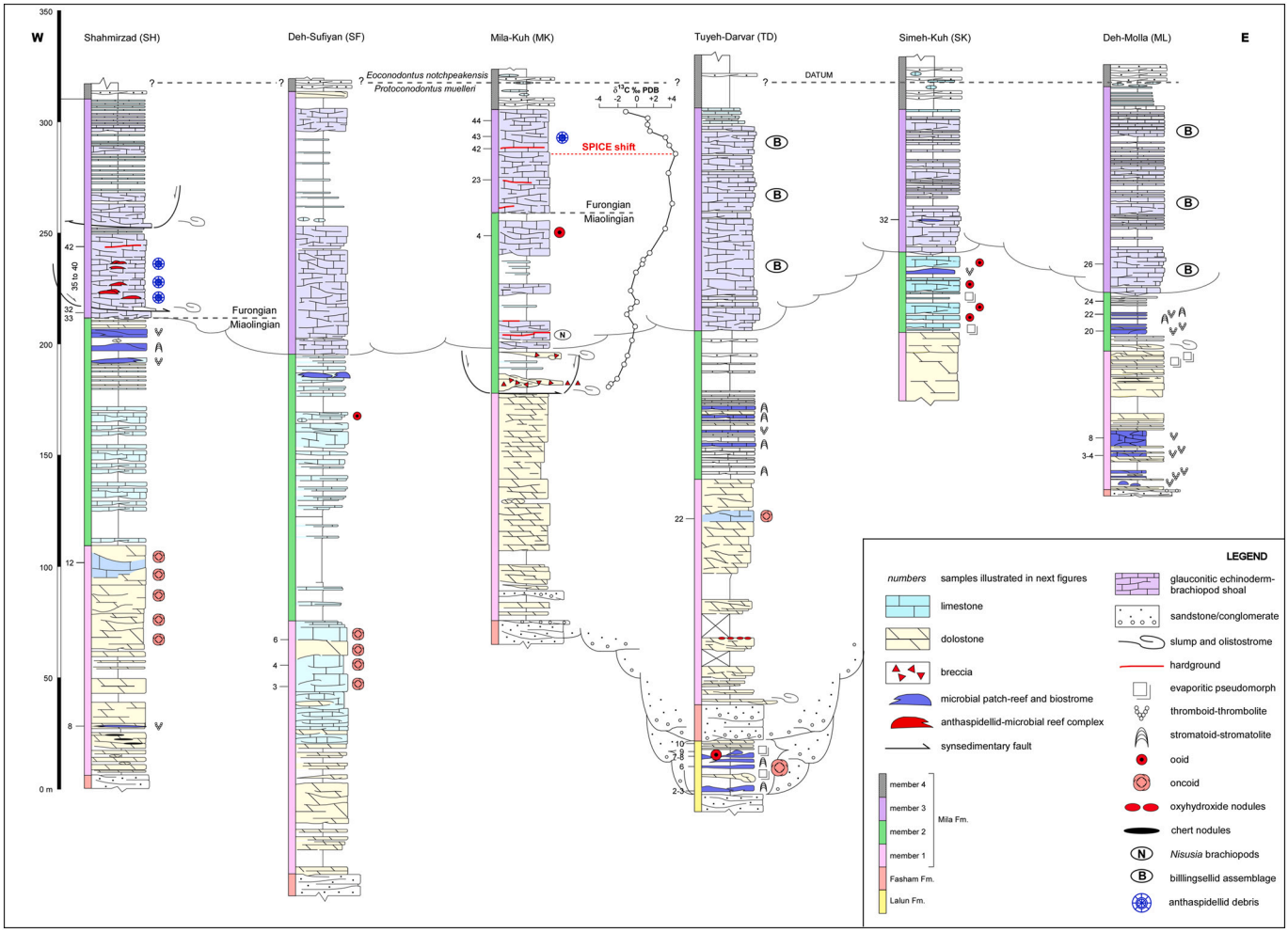


**Fig. 3.** Stratigraphic correlation of study sections organized in a W to E arrangement.

and *Hyrcanostrophia*, and tetralobulid *Palaeostrophia*) are abundant in the bioaccumulations that episodically punctuate the member (Popov et al., 2011, 2013). At Simeh-Kuh, the upper part of the member commonly contains linguliformean (phosphate-walled) brachiopods, such as the genera *Dactylotreta*, *Dictyonina*?, *Ottenbyella*, *Sadracarta*, *Siphonobolus* and *Tapuritreta* (Popov et al., 2009). The only published record of conodonts includes the paraconodonts *Rotundoconus* and *Westergaardodina*, and the possible presence of the euconodont *Protoconodontus* in the topmost part of the unit at Simeh-Kuh (Jahangir et al., 2016). The base of the overlying Member 4 is marked by the occurrence of shale/sandstone alternations, which display the first occurrence of *Proconodontus muelleri*, the nominal taxon for the earlier (but not earliest) Furongian euconodont zone (Jahangir et al., 2016) (Fig. 3).

## 3. Material and methods

Stratigraphic study and rock sampling were carried out through six measured sections located in the vicinity of Shahmirzad, Deh-Sufiyan, Mila-Kuh (stratotype), Tuyeh-Darvar, Simeh-Kuh and Deh-Molla villages (Figs. 1B, 3). All of them are located within the tectonostratigraphic Damghan Domain (Álvaro et al., 2022; Ghobadi Pour et al., 2022), on the southern foothills of the eastern Alborz Mountains.

One hundred and twenty sedimentary rock samples were selected for petrographic study. Carbonate thin-sections were stained with potassium ferricyanide and Alizarin Red S to recognize ferroan calcite, calcite and dolomite. Mineralogical identification was based on transmitted and reflected light microscopy and scanning electron microscopy (SEM) equipped with an energy-dispersive X-ray analyzer (EDX). The chemical composition of selected minerals was determined with a back-scattered electron (BSE) detector. SEM analysis was accomplished using a JEOL JSM-6400 fitted with an Oxford Instruments D6679 detector, with a high resolution of 3.5 nm at 25 kV, at Museo Nacional de Ciencias Naturales (MNCN), Madrid. Back-scattered (BSE) imaging and energy-dispersive X-ray spectrometry (EDS) analyses were obtained by SEM with the following measurement conditions: accelerating voltage 20 kV, beam current 1–2 nÅ and a counting interval of 50 s; analytical results display a relative error of ±5 to 7 %.

The Raman spectroscopy technique (confocal Raman microscopy, Thermo Fisher DXR spectrograph) of MNCN was used to characterize carbonaceous material on thin section. The light at 532 nm of a frequency doubled Nd: YVO4 DPSS solid laser (maximum power 30 mW) was used for excitation. Spectral data were evaluated with Thermo Scientific OMNIC Series Software. The Raman spectral signal of kerogen is recorded in a 'first order' region between 1000 and 2000 $cm^{-1}$ and a 'second order' region between 2000 and 3500 $cm^{-1}$. Bands in the second order region are generally hidden by fluorescence for low mature samples (Beyssac et al., 2002), and were not observed in this study. The interference due to high fluorescence caused by the diffuse presence of hydrogen and residual mineral matter was removed by a baseline subtraction procedure to accurately identify peaks in broad and overlapping bands (e.g., Ou et al., 2025), where baseline points at 1100 and 2000 $cm^{-1}$ were fixed for all the spectra. After removal of the background, the deconvolution of the averaged Raman spectra was performed by using computational software Peak Resolve (OMNIC Thermo Fischer). A

Lorentzian profile was employed for the band fitting, as it reduces the degree of freedom of the system, facilitating convergence (Lahfid et al., 2010). The fitting was adjusted to a four bands model, as search for the D2 band proved fruitless due to the low diagenetic degree recorded in the studied carbonates.

## 4. Representative microbial and microbial-metazoan reef complexes and bioaccumulations

Six main up-building phases are distinguished below (Figs. 2–3). The term 'reef' is used when the frame-building fabrics are dominated by peloidal, clotted (thromboid) and laminated (stromatoid) textures, rather than homogeneous mud. The fabrics correspond to 'Frame Reefs' *sensu* Riding (2002), in which in place skeletons (including calcified microbes) are in contact and microbial clotted-peloidal fabrics are

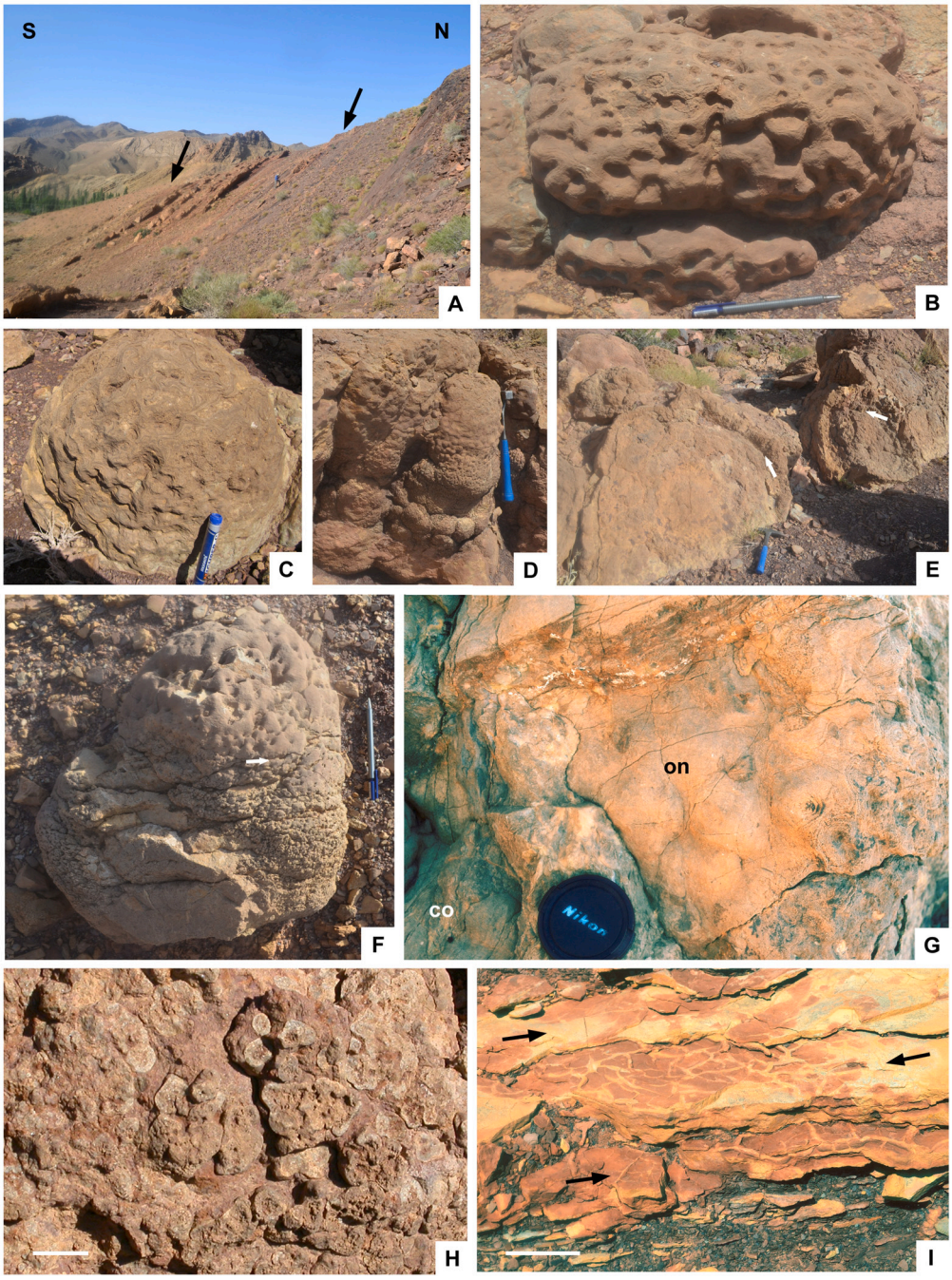


**Fig. 4.** Field aspect of characteristic facies associations from the Tuyeh-Darvar microbial reef complex. A. Landscape of a southern hillside to the east of Tuyeh-Darvar village with arrowed base (right) and top (left) of the upper member from the Lalun Formation. B–D. Vase-shaped domal stromatolites with cerebroid to knobby tops, separated by inter-reef oncoidal infills; B and C in level TD6, and D in TD9 (stratigraphic settings in Fig. 3). E. Top of a microbial reefal complex showing partial weathering and erosion of an uppermost columnar-shaped stromatolitic cap, underlain by a network of subparallel cracks (arrowed); TD9. F. Isolated stromatolitic patch-reef with vertical gradation (arrowed main contact) from planar crinkly to domal-cerebroid top; TD8. G. Core (co)-oncoidal (on) flank contact of a patch-reef; TD7. H. Field aspect of weathered pisoids and aggregates capping and flanking a stromatolite bioherm; TD2. I. Mud-cracked silty dolostone interlayers; TD3; scale bars = 2 cm (H) and 5 cm (I).

considered as microframe structures, typical of Cambrian buildups. The term 'patch-reef' refers to isolated pillow-shaped masses ranging in size from 0.2 to 2 m across and 0.2 to 1 m high (e.g., Álvaro and Debrenne, 2010). They can occur linked as clusters that coalesce vertically and laterally to form reef-complexes with composite geometries.

### 4.1. Microbial reef complex, late Cambrian Epoch 2

The upper member of the Lalun Formation exhibits, on a southern hillside to the east of Tuyeh-Darvar village (Figs. 1B, 3, 4A), microbial patch-reefs and bioherms interbedded with variegated marlstones and shales. The targeted member, 26 m thick, is sandwiched between two sandy shoal complexes, lithostratigrahically assigned to the lower member of the Lalun Formation and the Fasham Formation. The lower 20 m of the upper member display isolated patch-reefs and compound reefal complexes (Fig. 4B–F). Each build-up, with broad domes 0.5 to 2 m across, stands in stark relief due to the preferential weathering and erosion of the surrounding burrow-mottled marlstones and shales. The larger composite build-up is 8 m wide at the base and 2.2 m high. Most patch-reefs developed on a grainy base, composed of centimetre-thick oncoidal to intraclastic packstone and calcarenite layers. They are dominantly flanked and topped by packstone interbeds rich in oncoids (coated grains with microbial or algal growth, 0.5–2 mm in diameter; Fig. 4G), pisoids, (> 2 mm in diameter; Fig. 4H), radial and concentric ooids, aggregates and intraclasts. The core facies grades vertically from planar lamination to domal shapes and, locally, columns (Fig. 4F). Their texture is crinkly to wavy, locally interrupted by peloidal and intraclastic interlayering. The stromatolitic banding, visible at the naked eye, largely reflects variations in fenestral porosity (Fig. 4F). Some stromatolite caps, commonly separated from their lower reefal part by networks of cracks (Fig. 4E), show knobby to cerebroid surfaces occupying the uppermost band of the reef complex (Fig. 4B–C). Maximum topographic relief on the branching knobs is 2–6 cm. The reefal interbeds are punctuated by centimetre-thick low-angle sets rich in ooids and

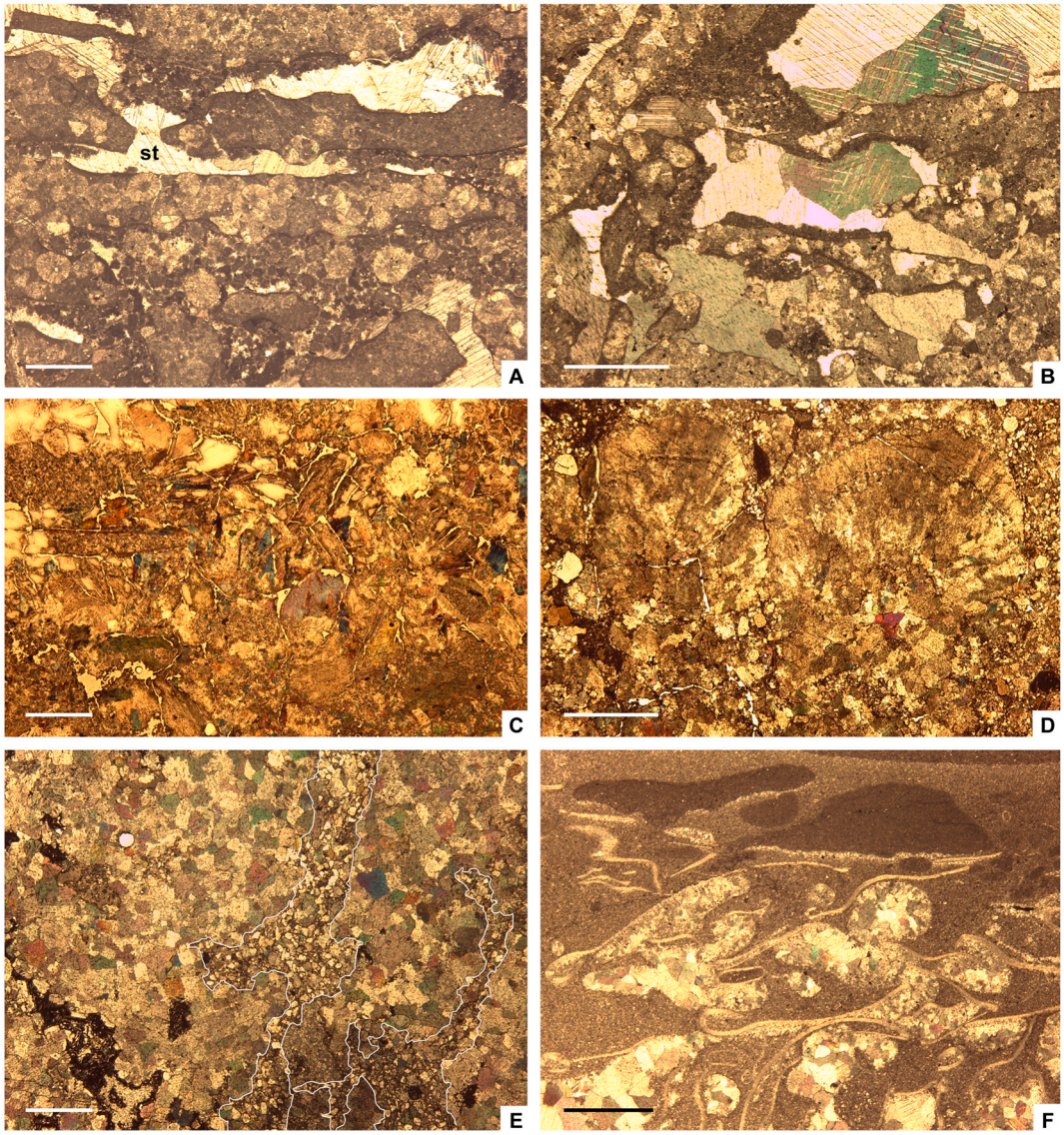


**Fig. 5.** Petrographic photomicrographs from the Tuyeh-Darvar microbial reef complex. A. Ooidal-peloidal-intraclastic packstone with interparticulate pores occluded with blocky calcite cements (st: stromatactis-like pore); level TD8 (stratigraphic setting in Fig. 3). B. Jigsaw-type breccia rich in intraclastone packstone clasts with distinct interparticulate pores infilled with blocky calcite cement; TD8. C. Subrectangular-shaped pseudomorphs after gypsum forming a single interlayer; TD9. D. Two fans of neomorphosed calcite crystals maintaining their original acicular morphologies; TD3. E. Subvertical fissuring infilled with silty calcite to dolomite, sourced from overlying siltstone layers; TD7. F. Wackestone rich in muddy intraclasts and trilobite sclerites, underlain by shelter pores progressively occluded with bladed and equant calcite crystals; TD10. Scale bars = 1 cm (A, C–F) and 500 μm (B).

intraclasts (Fig. 5A–B) and burrow-mottled, thin-bedded siltstone pervasively affected by desiccation cracks (Fig. 4I) with intraclastic lags, and locally interbedded with lozenge-shaped evaporitic pseudomorphs (Fig. 5C), synaeresis cracks and millimetre-thick laminites rich in microbially induced sedimentary structures (MISS; see Noffke et al., 2022). Some carbonate interbeds, up to 20 cm thick, comprise millimetre-sized crystalline fans and hemispheres (Fig. 5D) that are laterally linked to stromatolitic crusts. They are made up of crystals of neomorphosed calcium carbonate that display acicular morphologies with blunt terminations. Crystal fans may occur as isolated patches but they may also coalesce laterally. All the reported carbonates are commonly contorted, slump-folded and crosscut by millimetre- to centimetre-wide, steeply dipping to subvertical fractures forming fissure-fill networks (Fig. 5E) encased in an extensively recrystallized

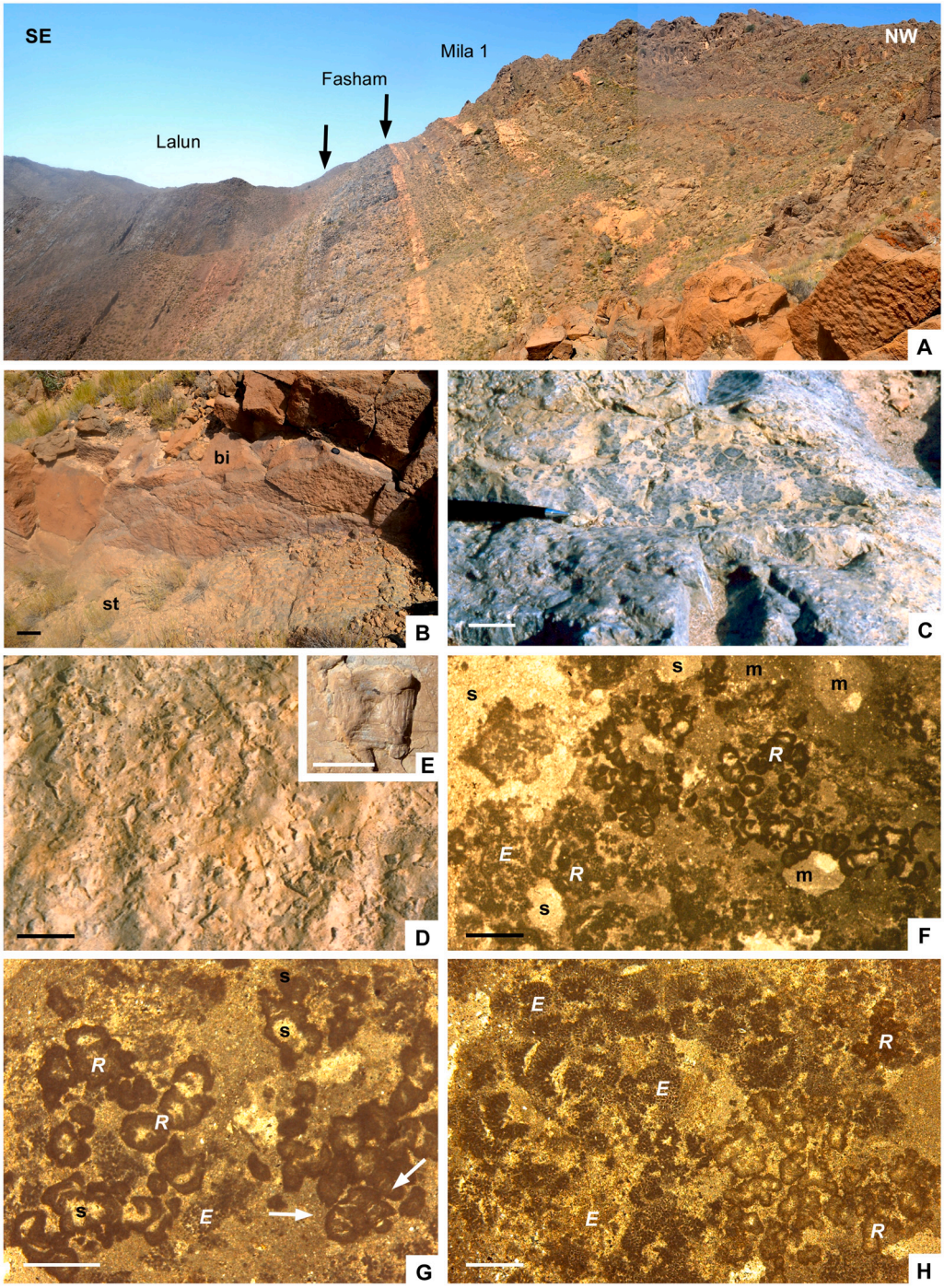


**Fig. 6.** Field aspect of facies associations and petrographic photomicrographs from back-barrier thromboid patch reefs of Mila Member 1 at Deh-Mola. A. Southern hillside to the south of Deh-Molla village showing the characteristic green-orange-ochre bands, with arrowed lithostratigraphic contacts. B. Orange-stained cross-stratified set (st) overlain by an ochre thromboid biostrome (bi); level ML3 (stratigraphic setting in Fig. 3). C. Detail of the former thromboid biostrome top displaying centimetre-scale *Renalcis* bushes; ML4. D. Top of a small-scale cycle covered by halite casts; ML8. E. Detail of former surface with a hopper-faced cube of halite pseudomorph; ML8. F–H. Thin-section photomicrographs of a thromboid patch-reef with networks of *Renalcis* (R) and *Epiphyton* (E) bushes surrounded by a silty microsparitic matrix punctuated with interparticle porosity occluded with muddy matrix (m) and sparry cements (s), and intraparticle clotted pores with diffuse internal layering (arrowed); ML3. Scale bars = 10 cm (B), 2 cm (C–D), 0.8 mm (E), and 500 μm (F–H).

host rock (Fig. 5E). Fracture porosity is filled with wall-rock angular clasts and brownish-stained silty grains rich in monocrystalline quartz and subsidiary feldspar. Some fracture walls are lined with crusts of sparry calcite. Their crystals vary significantly in size and morphology, from submillimetre-thick blocky to millimetre-thick coarse crystalline mosaics. Pockets of jigsaw-type breccia comprise clast fragments that are slightly displaced from their original wall position. Finally, the upper 6 m of the upper member, composed of carbonate/shale bedded alternations, display saddle to sparry mosaics of dolomite that have deleted primary textures. Some undolomitized interbeds, however, consist of intraclastic to bioclastic wackstones to packstones rich in disarticulated trilobite sclerites (Fig. 5F).

#### 4.1.1. Interpretation

The upper member of the Lalun Formation, underlain and overlain by sandy shoal complexes interpreted as tidally influenced estuarine environments (Bayet-Goll et al., 2018, 2021), would represent back-barrier deposits. The lagoon episodically recorded subaerial exposure and evaporitic conditions, recognized by the record of mudcracks and lozenge-shaped pseudomorphs after gypsum. The contorted and slumped preservation of some patch-reefs, as well as their generalized fissured aspect, reflect unstable substrates affecting both partly unconsolidated and rigid build-ups. This controlled the growth of planar to domal and columnar microbial patch-reefs and bioherms, underlain, flanked and overlain by intraclastic, oncoidal and pisoidal lenses. Compound reefal complexes reaching metre-scale reliefs only developed over stabilized substrates. Polygonal cracking and MISS are common in microbial mats accumulating in semiarid climates (Noffke et al., 2001; Smith et al., 2021). Club-shaped and cerebroid stromatolites from Shark Bay, western Australia, are known to thrive in semi-restricted waters (Collins and Jahnert, 2014).

Semi-closed lagoon episodes recorded microbial activity under conditions ranging from high aridity to hypersalinity, episodically interrupted by incursions of marine water. The trilobite-rich packstone interbeds of the upper part would reflect sporadic shoal-backward storm-induced washovers. In contrast, the precipitation of crystalline carbonate fans reflects seafloor-encrusting marine cements, where the neomorphosed calcite crystals point to possible aragonite precursors. No archaeocyaths are recognized, and some undetermined remains assigned to these sponges by Lasemi and Amin-Rasouli (2007) may be reinterpreted as mud-coated intraclasts, single radial and concentric ooids, composite aggregates and pisoids, stromatoclasts, dendritic thromboids or cements and cracked stromatolites.

### 4.2. Back-barrier thromboid patch-reefs, Miaolingian

Despite the generalized dolomitization recorded in Member 1 throughout the eastern Alborz Mountains, some limestone interbeds can be recognized south of Deh-Mola village (Figs. 2–3). There, the member comprises cycles of three repeated facies, 6 to 17 m thick. Their successive green, orange and ochre colours give the outcrop a distinctive banded appearance (Fig. 6A): (i) the green interbeds, up to 8 m thick, are structureless shales and marlstones with subordinate centimetre-scale, laminated and locally burrowed, clayey/silty couplets; (ii) the orange limestone and dolostone interbeds, up to 9 m thick, consist of amalgamated low-angle to trough cross-bedded sets, with wave-ripple lamination and wave ripples on bed tops, broadly composed of sparry to ooidal packstone to grainstone (Fig. 6B); the lenticular sets are locally scoured and capped by mud-cracked shale laminae, with curled up edges and rich in crystal pseudomorphs recognized as simple cubes (Fig. 6D), hopper-faced cubes (Fig. 6E) and their intergrowths; and (iii) the ochre to brownish limestone interbeds show vertical gradation from lower amalgamated nodules to upper lenses of decimetre-scale thromboid patch-reefs and biostromes (Fig. 6C), in some cases, capped by dolomitized crust-like laminites, up to 4 cm thick and locally mudcracked.

The frame-building framework of the brownish limestone interbeds (iii) consists almost exclusively (~90 % in thin-section) of clotted textures, locally encasing minor bioclast debris and large (up to 3 mm) pores that overall constitute up to 15 % of the whole framework. Porosity is irregularly distributed and infilled by either non-clotted micrite (currently recrystallized or dolomitized) or microsparite to sparite (Fig. 6F–G). Clots, 60 to 800 μm in size, are subrounded to irregular, elongate to equant patches of cryptocrystalline calcite encased in a more coarsely crystalline calcite mosaic (Fig. 6F–G). Some clots display irregular and diffuse internal layering, visible by differences in the dark/light intensities (arrowed in Fig. 6G), produced by modifications in the micrite/peloid packing density (peloid refers here to granular micritic aggregates of uncertain origin). They form loosely coalesced, botryoidal clusters, interconnecting branches and layered crusts, up to 2 cm across, locally surrounded by geopetal pockets. Microscopic voids between clots are filled with sparry calcite, small cement-filled fenestrae and pseudospar (Fig. 6F–H). Interconnected to amalgamated clotted bodies, with walls about 5–20 μm thick and micritic centres, resemble *Renalcis* forms (Fig. 6F–G). Bushy forms resembling *Epiphyton* calcimicrobes occur as scattered, grape-like and branching (with acute angles between branches), discontinuous to continuous rods (Fig. 6H). Other straight filaments form laminated networks of unbranching, subparallel bunches to somewhat radiating micritic fans, where individual filaments are 10–30 μm in diameter and up to 400 μm long (Fig. 7A). Amalgamated subparallel crusts (Fig. 7B) show crude interlayers of irregular meshworks and clotted pockets.

#### 4.2.1. Interpretation

The three aforementioned facies (i to iii) are arranged as shallowing-upward small-scale cycles. Their bases are flooding surfaces and their tops discontinuities marked by the development of uneven scouring and hardground surfaces, in some cases emphasized by microbial crusts. From bottom to top, the cycles start with an initial phase of rapid deepening, marked by partly burrowed green shales deposited on offshore-dominant substrates, prograding ooidal to sparry shoals, and back-barrier (protected) thromboid patch-reefs finally capped by peritidal microbial laminites. Thromboid patches and biostromes consisted mainly of clotted structures, with calcite cements later filling centimetre-scale voids to lithify the framework. Microbial processes comprise calcification, trapping and binding of intraclasts. The thromboid texture is emphasized by micritic (uniform, clotted and peloidal) meshworks with unusual or absent allochthonous silt-sized grains, pointing to almost exclusively autochthonous particles. Halite precipitation may be related to episodes of increasing salinity in an arid setting, where circulation was somewhat occasionally restricted.

### 4.3. Oncoidal-pisoidal accumulations punctuated by microbial crusts, Miaolingian

Oncoid-pisoid rudstone limestone and dolostone interbeds form a significant part of Member 1 in the Shahmirzad, Deh-Sufiyan and Tuyeh-Darvar sections (Fig. 3). Oncoidal-pisoidal lenses, up to 0.4 m thick, occur interbedded with low-angle cross-laminated sets punctuated by mud-cracks and microbial crusts, and subsidiary tepee structures and centimetre-thick, ooid-oncoid-intraclastic grainstone lenses (Fig. 7C). Oncoids and pisoids, both spherical and flattened (subparallel to bedding plane), commonly display lobate to elliptical shapes and sharp outlines (Fig. 7D), and commonly account for 20–60 % of sample volume. The texture is mainly grain-supported, and the interstitial matrix consists of sand-sized carbonate grains mixed with siliciclastic debris. Several nuclei can be recognized, such as peloids, carbonaceous lumps, intraclasts and bioclasts (mainly trilobite sclerites and brachiopod valves), although some of them lack distinct nuclei (i.e., full cortex unlaminated oncoids *sensu* Han et al., 2015) (Fig. 7E–H). They exhibit a cortex composed of well-defined concentric laminae of variable thickness. Crinkly lamination is locally emphasized by microbial filaments mimicking *Girvanella* remains.

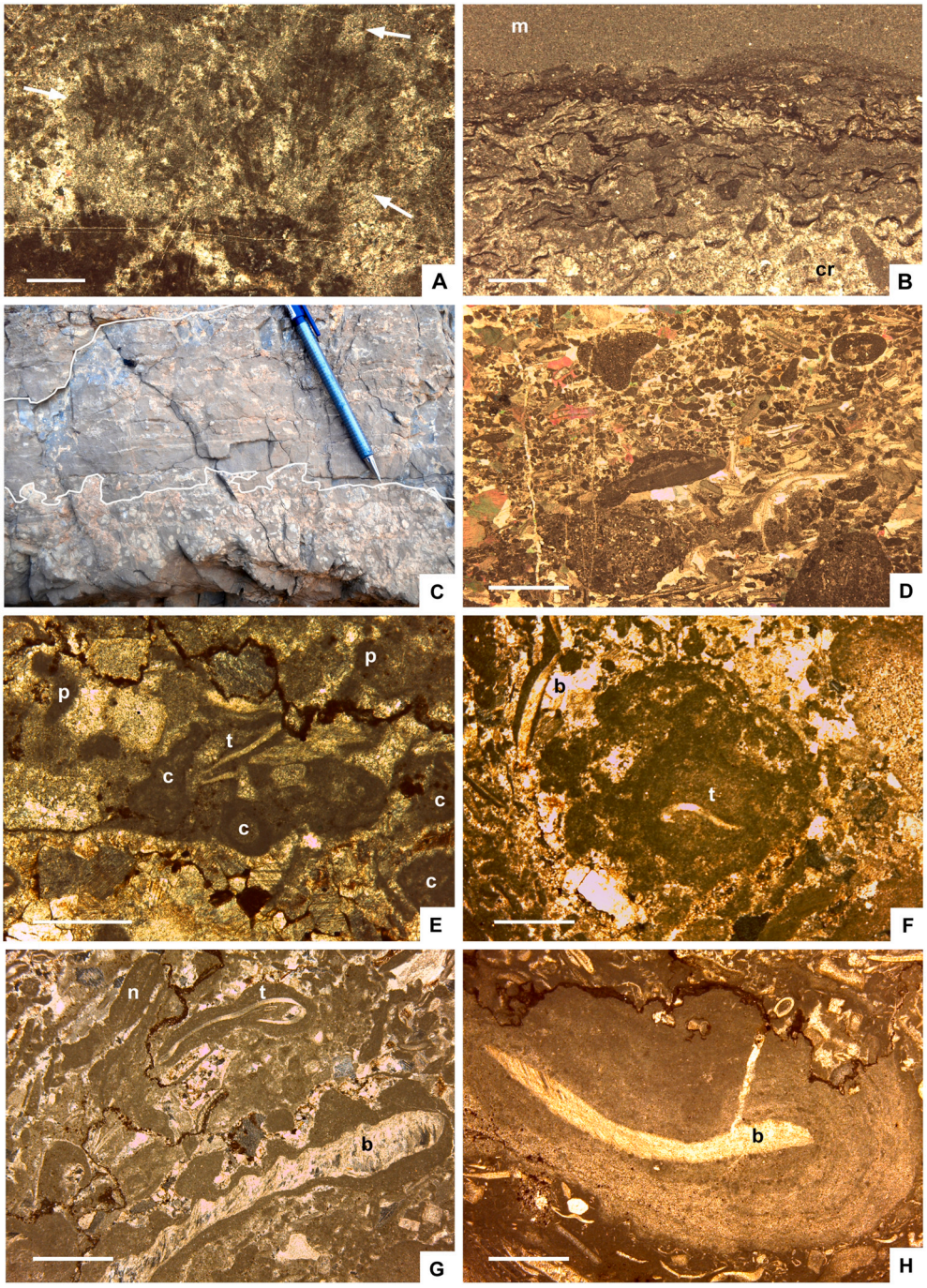


**Fig. 7.** Field aspect of facies associations and petrographic photomicrographs. A. Thin-section photomicrograph of a thromboid texture of Mila Member 1 at Deh-Mola showing a superposition of radiating fans composed of tubular filaments mimicking *Epiphyton* networks; level ML3 (stratigraphic setting in Fig. 3). B. Petrographic photomicrograph of the top of a shallowing-upward cycle illustrating a lower ooidal-intraclastic grainstone crust (cr), encrusted by stromatolitic mats affected by solution seams, finally onlapped by a mudstone (m), which forms the beginning of the overlying cycle; SH8. C. Oncoid-pisoid dolomitized rudstone interbeds separated by erosive discontinuities (lined); Member 1 at Tuyeh-Darvar; TD22. D. Thin-section photomicrograph of an oncoidal-peloidal packstone; Member 1 at Deh-Sufiyan; SF3. E–H. Detail of some pisoids exhibiting different nuclei types: b- brachiopod valve, c- carbonaceous lump, n-lack of nuclei, p- peloid, and t- trilobite sclerite; SF6. Scale bars = 500 μm (A–B, D–E) and 2 mm (F–H).

#### *4.3.1. Interpretation*

The pisoid components reflect partly restricted conditions, potentially associated with shallow, warm and moderately agitated waters (e.g., Torromé et al., 2022) episodically submitted to subaerial exposure. Episodic marine influence is indicated by the oncoid-pisoid interlayering with shelly coquinas (e.g., Védrine et al., 2007). The virtual absence of micrite suggests a fairly high-energy setting linked to nearshore substrates recording oncoidal-dominant low-angle shoal systems. Development of the crinkly lamination in oncoids and pisoids was triggered by successive growth layers of the cortex, which suggest permanent high-energy conditions and active microbial encrustation. The episodic flourishing of microbial communities may be related to increasing nutrient pulses, potentially highlighting the onset of stratigraphic diastems (Álvaro and Clausen, 2006).

### 4.4. Open-sea stromatoid and thromboid patch-reefs, Miaolingian

In the absence of ribbon facies associations (see Bayet-Goll et al., 2018, 2021), Member 2 at Deh-Mola and Sime-Kuh displays rhythmic or repetitive strata, 8–22 m thick, composed, from bottom to top, of (i) green structureless shales and marlstones, up to 3 m thick, locally interbedded with burrowed, clayey/silty couplets and chaotic clast- to matrix-supported, contorted interbeds; (ii) plano-convex patch-reefs, up to 0.9 m thick, composed of either laminated or clotted boundstones; and (iii) dolomitic laminites, less than 0.3 m thick, containing evaporitic pseudomorphs.

Planar domal and columnar, stromatolitic boundstones (Fig. 8A–B)

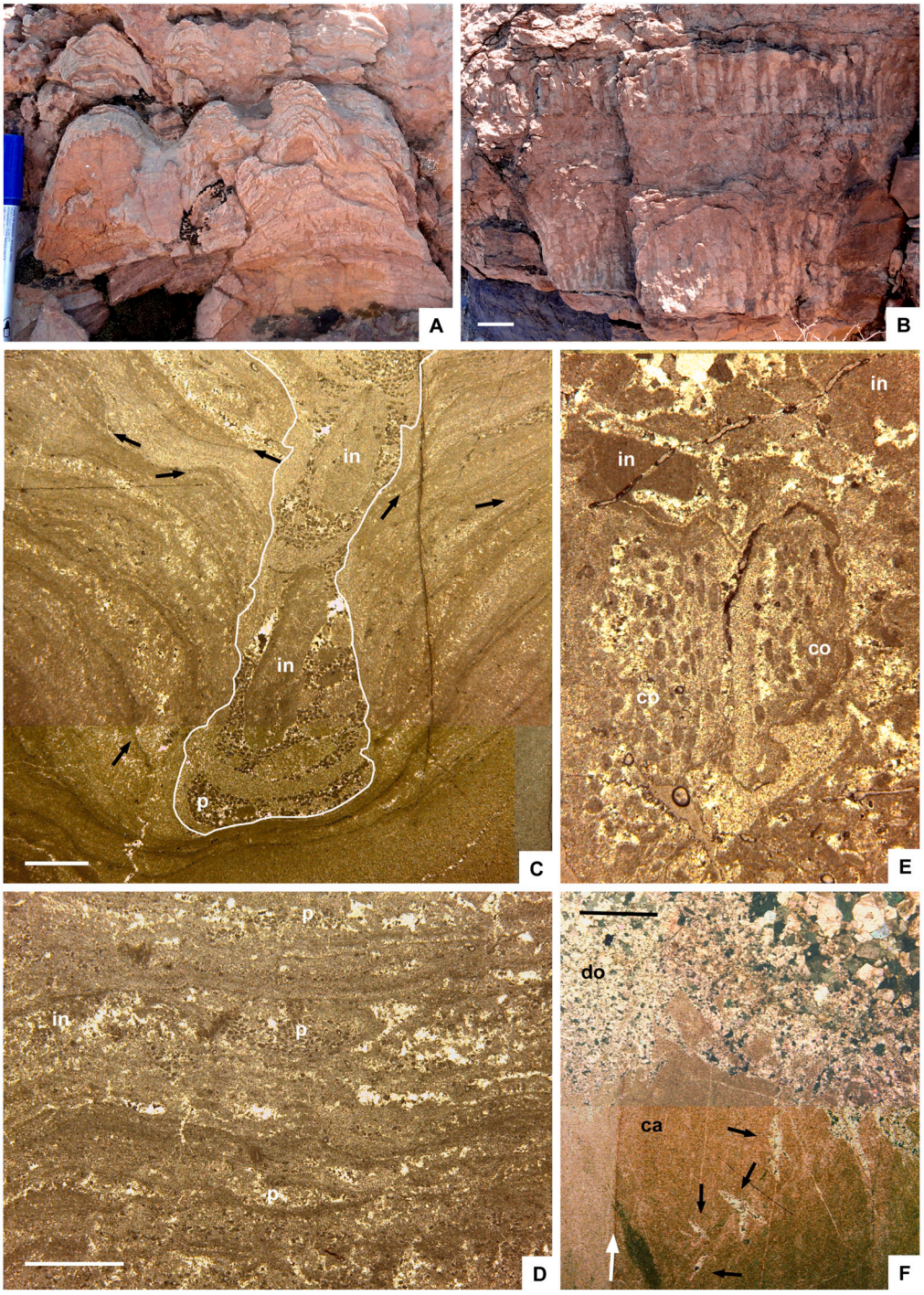


**Fig. 8.** Field aspect of facies associations and petrographic photomicrographs of stromatolites from Member 2 at Deh-Molla. A. Amalgamation of domal stromatolitic limestones with distinct synoptic relief; level ML20 (stratigraphic setting in Fig. 3). B. Alternation of dolostone interbeds, two of them with columnar stromatolites; ML22. C. Thin-section photomicrograph of two laterally linked domal stromatolites separated by scouring infill (lined) rich in peloids and intraclasts; onlapping contacts of smooth thickening laminae, arrowed; ML22. D. Detail of fenestral pores and peloidal-intraclastic interlaminae; ML22. E. Detail of a V-shaped mudcrack infilled with peloids, intraclasts and composite (polyphase) clasts; ML22. F. Top of shallowing-upward cycle showing upsection dolomitization (white arrow marks the boundary of Alizarin Red S staining) and increase of crystal size, linked to the record of lozenge-shaped pseudomorphs after gypsum (black arrows); ML22. Abbreviations: ca- calcite, co- composite clasts, do- dolomite, in- intraclasts, p- peloids. Scale bars = 1 cm (B), 2 mm (C–D, F), 1 mm (E).

comprise uniform to crinkly laminated micrite/microspar couplets. Centimetre-scale domes and columns are typically 2–12 cm in diameter, with circular to slightly ovate cross-sections, and up to 12 cm high. Carbonate allochems, such as peloids, intraclasts and composite clasts, form a substantial portion of the laminae (up to 35 % of volume), as either disseminated grains or distinct laminae. Domes and columns, with synoptic reliefs, comprise well-defined laminae, generally less than 5 mm thick (Fig. 8C–E). In some cases, closely spaced adjacent domes and columns hardly coalesced to form single, larger and composite, domal structures. Sustained thickening of laminae between domes gradually resulted in a gradual upward reduction in synoptic relief. Laminar inheritance is distinct, but scouring surfaces affect both laminar

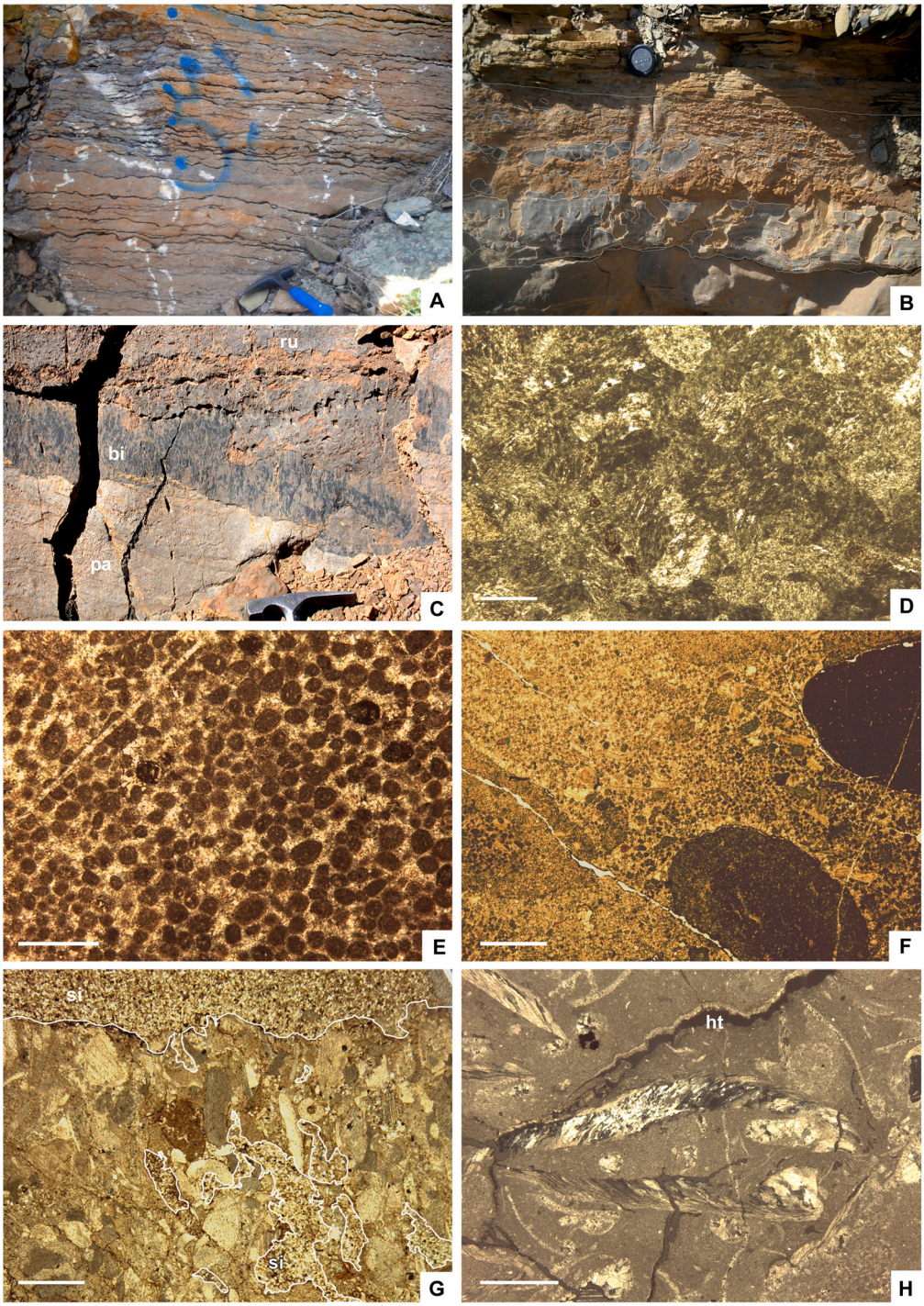


**Fig. 9.** Field aspect of facies associations and petrographic photomicrographs from the shell beds that characterize Member 3 of the Mila Formation. A. Typical pinkish echinoderm-rich packstone to grainstone layers bounded by reddish shale-rich solution seams and stylolites; level SH32 (stratigraphic setting in Fig. 3). B. Scouring contacts separating low-angle laminated, echinoderm-rich packstone and breccia interbeds; SH33. C. Digitate thromboid biostrome (bi) encrusting a packstone interbed (pa) and scoured by a brachiopod-rich rudstone (ru); SK32. D. Detail of former thromboid showing a network of digitate fans, encrusting each other; SK32. E. Ooidal-peloidal grainstone set; MK4. F. Calcarenite of unselected intraclasts, ooids, peloids and oncoids; ML26. G. Top of Member 3 showing subvertical cracks and fissures infilled by same facies than overlying siltstone (si); MK23. H. Rhynchonelliform-rich wackestone to rudstone with articulated and disarticulated valves, locally encrusting a hematite-rich hardground (ht); MK44. Scale bars = 250 μm (D) and 500 μm (E–H).

amalgamation and sharp horizontal changes in thickness and columnar width (Fig. 8C). Fenestrae range in size from 0.1 to 5 mm in diameter. They currently follow the orientation of underlying and overlying laminae, and exhibit subspherical morphologies. Inter-columnar space is filled with microsparite to pseudosparry carbonate, aggregate grains and rip-up stromatoclasts (Fig. 8D). Some laminae are mudcracked, include small folds and roll-up microstructures, and/or capped by centimetre-thick breccia interlaminae (Fig. 8E) with pores infilled with reddish siltstone. The uppermost part of the cycles displays dolomitic crinkly laminites, sparsely fenestral and with internal alternations of dolosparite and dolomicrosparite, locally linked to lozenge-shaped pseudomorphs (Fig. 8F). Thromboids display similar textures, fabrics and patch-reef geometries to those reported in Section 4.2, and will not be repeated here.

#### 4.4.1. Interpretation

The three aforementioned facies (i to iii) reflect shallowing-upward small-scale cycles. The microbial patch-reefs flourished, not in protected back-barrier settings (see Section 4.2), but under open-marine, subtidal conditions, where the influence of invertebrate grazers and burrowers, which widely developed on the distal marly-shaly substrate, was somewhat reduced. No intermixed laminated/clotted textures have been recognized. Development of spatially restricted patch-reefs, rather than laterally continuous biostromes, reflects recurrent environmental stress imposed by evaporitic conditions and substrate instability, evidenced by mudcracks, halite and gypsum pseudomorphs, and rip-up clasts. Patch-reefs developed fringing peritidal environments, locally recording arid evaporitic precipitation representing the uppermost part of shallowing-upward cycles.

### 4.5. Shell beds generated by pelmatozoan-rhynchonelliformean meadows, Miaolingian and Furongian

This facies association occurs interbedded in the upper part of Member 2 at Sime-Kuh stratotype (Holmer et al., 2019) and forms the main part of Member 3 throughout the eastern Alborz Mountains (Fig. 3). It consists of light grey to pinkish, variably glauconitic, thin- to medium-bedded limestones alternating with subsidiary shales (Fig. 9A). Scouring surfaces capped by breccia lags are common (Fig. 9B). Shell beds are also locally punctuated by centimetre- to decimetre-thick thromboid crusts (Fig. 9C–D) and anthaspidellid-microbial reef complexes (Furongian in time, see Section 4.6). Limestone strata are dominated by cross-bed sets, up to 1 m thick, with horizontal to low-angle laminae and hummocky cross-stratification, locally emphasized by clayey interlaminae, solution seams and stylolite surfaces (Fig. 9A). Their texture consists of packstone to grainstone rich in ooids, grapestones (or aggregates), oncoids and bioclasts (Fig. 9E–F). Subvertical fissures and cracks are abundant, and their fracture porosity is infilled with the same silty material (Fig. 9G). Echinoderm ossicles and brachiopod valves are volumetrically the most important skeletal constituents, reaching locally more than 80 % of the rock volume, whereas subsidiary components are mainly trilobites, hyoliths, linguliformean brachiopods, conodonts and palaeoscolecid sclerites (Peng et al., 1999; Wrona and Hamdi, 2001; Popov et al., 2011, 2013; Jahangir et al., 2016). Compositional analysis shows lateral variations in the skeletal association, ranging from pelmatozoan- to brachiopod-dominant shell pavements and accumulations. Shell beds are sharp-based and display low-angle planar cross-lamination. Skeletons are disarticulated to fragmented and commonly arranged as stacked, nested, imbricated and variably oriented shells. Some entirely preserved and partly articulated ossicle remains allowed the identification of vagile stylophorans (Member 2; Rozhnov and Parsley, 2017) and edrioasteroids (Member 2; Guensburg and Rozhnov, 2014). Reworked anthaspidellid debris is exceptional in Member 2 (see description in Section 4.6). Cementation occurs as sparry mosaics occluding intra- and interparticulate pores. Some allochems are enveloped by isopachous calcite cement, and the remaining porosity was occluded with both equant, medium, calcite sparry mosaics and geopetal peloidal and micritic sediment. The pelmatozoan fabric is locally punctuated by centimetre-thick pavements to decimetre-scale, poorly bedded to lenticular brachiopod rudstone interbeds (Fig. 9H). Brachiopods are preserved as both articulated and disarticulated valves, in some outcrops protruding from the weathered bedded surface as silicified brachiopod shells. Lenses display both poorly defined irregular morphologies and distinct sharp basal surfaces with abundant rhynchonelliform brachiopods preserved in life position. In Member 2, rudstone lenses of rhynchonelliform brachiopods are dominated by species of *Nisusia*, whereas those of Member 3 comprise species of *Billingsella* (endemic species) and *Palaeostrophia*, forming the so-called *Billingsella* Association (e.g., Tuyeh-Darvar; Popov et al., 2013). Matrix is a mixture of medium- to coarse-grained silt and sand grains, and fragments of valves and ossicles.

#### 4.5.1. Interpretation

The thin- to thick, cross-bedded bioclastic-ooidal-oncoidal deposits described above represent migrating shoal packages. The record of trough cross-bedding sets suggests deposition in high-energy (shoreface-dominant) environments. The storm imprint is evidenced by normally graded interbeds and overturned brachiopods. The generalized flat-shaped aspect of most intraclasts points to erosion from thin sheets of formerly lithified sediment. The sharp-based nature of some bio-accumulations, preservation of fragmented and disarticulated bioclasts, and relative rounding of allochem edges support physical abrasion and hydraulic concentration. The principal constituents of the shell beds include dispersed, parautochthonous components punctuated by clayey interlaminae.

Hydrodynamic packages formed through the growth and destruction of pelmatozoan-rhynchonelliformean meadows by wave and storm action. The coarsest skeletal fraction was left in place, whereas the smaller ossicles, valves and sclerites were redistributed by currents. Sandwaves appear to have formed and migrated across the seafloor, as evidenced by large, high- to low-angle, tabular-planar cross-beds. The faunal record is a mixture of both vagile and sessile epifaunal organisms. This suggests the substrate was episodically stable enough to be colonized by pelmatozoan eocrinoids (Rozhnov, 2015).

An interval of this facies association, 38 m thick, occurs interbedded in the upper part of Member 2 at Mila-Kuh section, and contains facies and sedimentary structures identical to those exhibited by Member 3. These interbedded pelmatozoan-rich shoals contain rhynchonelliform nisusioid brachiopods reflecting the episodic development of Miaolingian nisusioid thickets (Holmer et al., 2019), which were deposited above the wave base with moderate supply of siliciclastic material. The variably energetic substrate favoured the development of large thick-shelled rhynchonelliform brachiopods that were able to anchor strongly in the grainy substrate. Brachiopod rudstones reflect moderate-energy settings due to the low articulation ratio of valves, whereas echinoderm packstone to grainstone interbeds were deposited in more energetic substrates. The grainy substrate rich in brachiopod shells in turn offered hard substrates to pedicle-attached brachiopods, spiculate sponges, pelmatozoan echinoderms and microbial crusts, locally favouring thicket (and reefal, see Section 4.6) stability. Substrate played a major role in controlling brachiopod colonization as they selected early cemented (firmground, see Section 5) substrates with respect to grainy (packstone to grainstone) mobile substrates. The concept of ‘taphonomic feedback’, linked to live-dead interactions between shelly organisms, and their role in the evolution of benthic ecological communities (Kidwell and Jablonski, 1983), can be applied to these shell beds. Although no patch-reefs have yet been recognized embedded in Member 2, the record of interbedded parautochthonous anthaspidellid debris point to their episodic growth attempts.

### 4.6. Anthaspidellid-microbial reef complexes, Furongian

Reefal frameworks of Member 3 mainly lie along a N–S trending road cutting about 3 km of Shahmirzad village (Hamdi et al., 1995). The geometric relationships and outlines between individual and composite reefs and their surrounding pelmatozoan-rhynchonelliformean sets are visibly exposed along the road margin and creek (Fig. 10A). As illustrated by Álvaro et al. (2022), Member 3 is here crosscut by synsedimentary normal faults (Fig. 10A–B). Although tilted blocks display uplifted footwall and lateral hanging-wall blocks with offsets close to 6 m, scarps are not significantly fringed by slope-related debris. Frame-building fabrics occur dominantly as patches and larger bioherms, up to 2 m high and 6 m wide, on tilted hanging-wall blocks. They appear as single units interbedded with pelmatozoan-rhynchonelliformean lenses and reefal complexes of patches and bioherms stacked vertically (Figs. 10C–F, 11A). In plane section, individual patches are elliptical to asymmetric in shape. The individual reefs and complexes, as a whole, show no preferential orientation or elongation.

Reefal cores consist of mottled lithistid-bearing limestones (Figs. 11B–E, 12A–B) with skeletal walls and substrates mainly encrusted by intergrowths of *Girvanella* crusts (Kruse and Zhuravlev, 2008) (Fig. 12C) and subsidiary clotted textures that locally exhibit recognizable *Epiphyton* and *Renalcis* morphs (Fig. 12D–E). Sponges mostly display conical, thin-walled skeletons due to longitudinal subdivision form branching modules that compose the reefal framework (Figs. 11D, G, 12F–I). In some cases, the sponge individuals occupy about 50 % of the overall volume, with individual calyx diameter up to 1.2 cm, and heights up to 2 cm. Individual patches rest on centimetre-thick intervals of intraclastic packstone to oncoidal-pisoidal rudstone (Figs. 11A, F, 12J), and interfinger with adjacent inter-reef, limestone/shale alternations that, in turn, grade laterally into echinoderm- and brachiopod-rich accumulations (Fig. 11H) (see Section 4.5).

Micrite fills some irregular pores separating filaments and subrounded clots, somewhat preserving the original texture. Local modifications in the volume and shape of pores are probably linked to an inherited fenestral texture (Fig. 12C), which was subsequently modified during recrystallization. The growth of microbial clots and filaments resulted in a framework texture with the original porosity partly occluded with fibrous to bladed, calcite cement (up to 300 μm in size; Figs. 11G, 12E). Subsidiary shelly debris comprises echinoderm ossicles, fragments of brachiopod valves and trilobite sclerites. The inter-reef facies consists of reddish to greenish limestone interbeds, 5–15 cm thick, with shale interlayers. Inter-reef strata consist of wavy to nodular oncoidal rudstone alternating and grading laterally into packstone to grainstone rich in disarticulated and partly broken, calcite-walled brachiopods and echinoderm ossicles (Fig. 11E–H).

#### 4.6.1. Interpretation

The nucleation, growth and demise of anthaspidellid-microbial reef complexes in the vicinity of Shahmirzad was directly controlled by synsedimentary faulting. Aerial photographs and mapping, as well as drastic changes in lithofacies, reflect differential subsidence of fault-bounded blocks, with shell beds generated by pelmatozoan-rhynchonelliformean meadows and thickets mainly developed on shallower water, uplifted footwall blocks. In contrast, anthaspidellid-microbial isolated patch-reefs and reef complexes embedded in

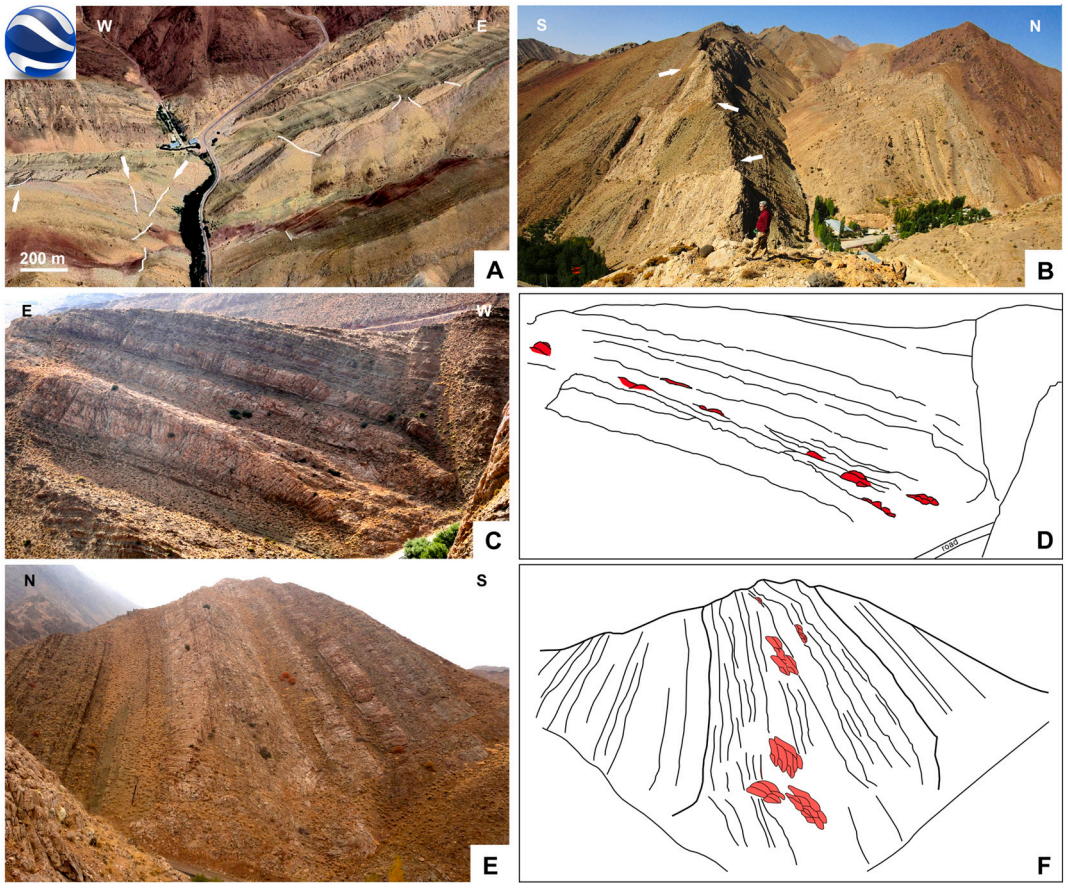


**Fig. 10.** Field aspect of Mila 3 Member strata in the vicinity of Shahmirzad displaying anthaspidellid-microbial reef complexes. A. Geological sketch on Google Earth image highlighting the unconformities and synsedimentary faulting (arrowed faults are sealed by overlying strata), north of Shahmirzad village. B. Western margin of the creek with arrowed foot-wall and hanging-wall blocks. C–D. Field image and sketch of Member 3 in a E–W transect with setting of isolated and amalgamated anthaspidellid-microbial patch-reefs. E–F. Similar arrangement in a transverse, N–S transect.

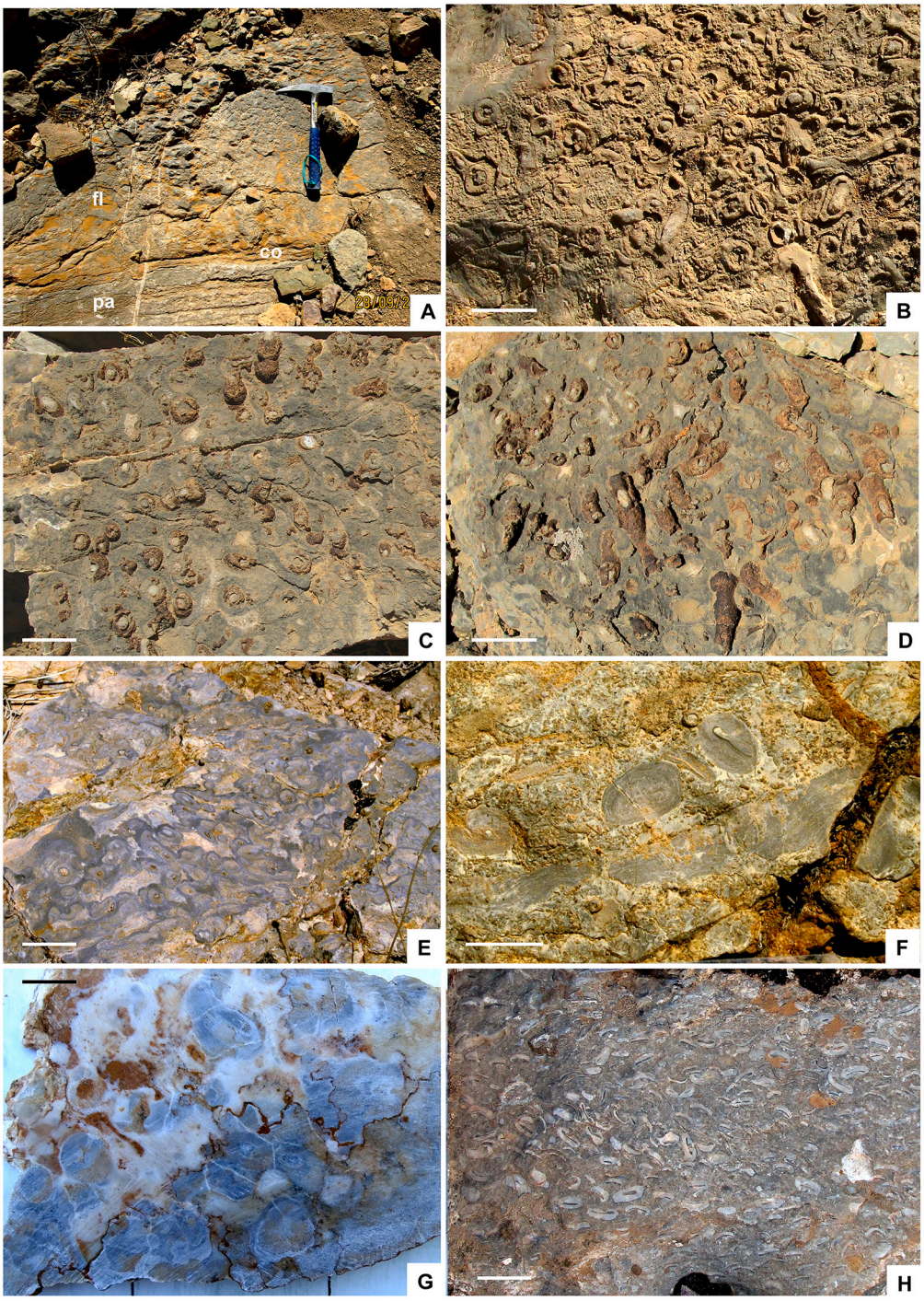


**Fig. 11.** Field aspect of the anthaspidellid-microbial patch-reefs. A. Single patch-reef (core, co) with oncoidal packstone (pa) base and flanks (fl). B–C. Upper surface of a biostrome displaying selective weathering of partly silicified *Rankenella* cups preserved in their original, upright growth orientation. D. Cross-section of a patch-reef flank rich in parautochthonous *Rankenella* cups, dominantly preserved parallel to stratification. E. Fresh cross-section of a core displaying *Rankenella* cups preserved in life position encrusted by grey zoned thromboids. F. Oncoidal-pisoidal-peloidal packstone forming the base of a single patch-reef. G. Polished slab of a reefal core sample showing transverse section of *Rankenella* cups, preserved in life position, with reddish silty microsparite infilling the space among cups and final occlusion of interparticulate porosity by calcite cement. H. Mixture of *Rankenella* cups (with dominated ellipsoidal section) and rhynchonelliformean valves forming a floatstone flank. Scale bars = 1 cm (B–F) and 2 cm (G–H).

pelmatozoan echinoderm-brachiopod shell beds (Section 4.5) dominantly established on deeper water, hanging-wall blocks. Reef complexes comprise stacked patches developed by their nucleation in close proximity. Development of microbial crusts and early-diagenetic cementation resulted in the development of build-ups with a positive synoptic relief, as well as distinct contacts between reef and inter-reef facies. Limestone flanks onlap the patch-reefs and are inclined off them, also supporting a primary positive topographic relief between the reef and inter-reef facies. Reefal growth took place episodically where and when bottom currents and/or waves were relatively weak. Build-ups were finally blanketed by current- and/or wave-winnowed bio-accumulations. Reefal bases consist of oncoidal debris and stromatolitic

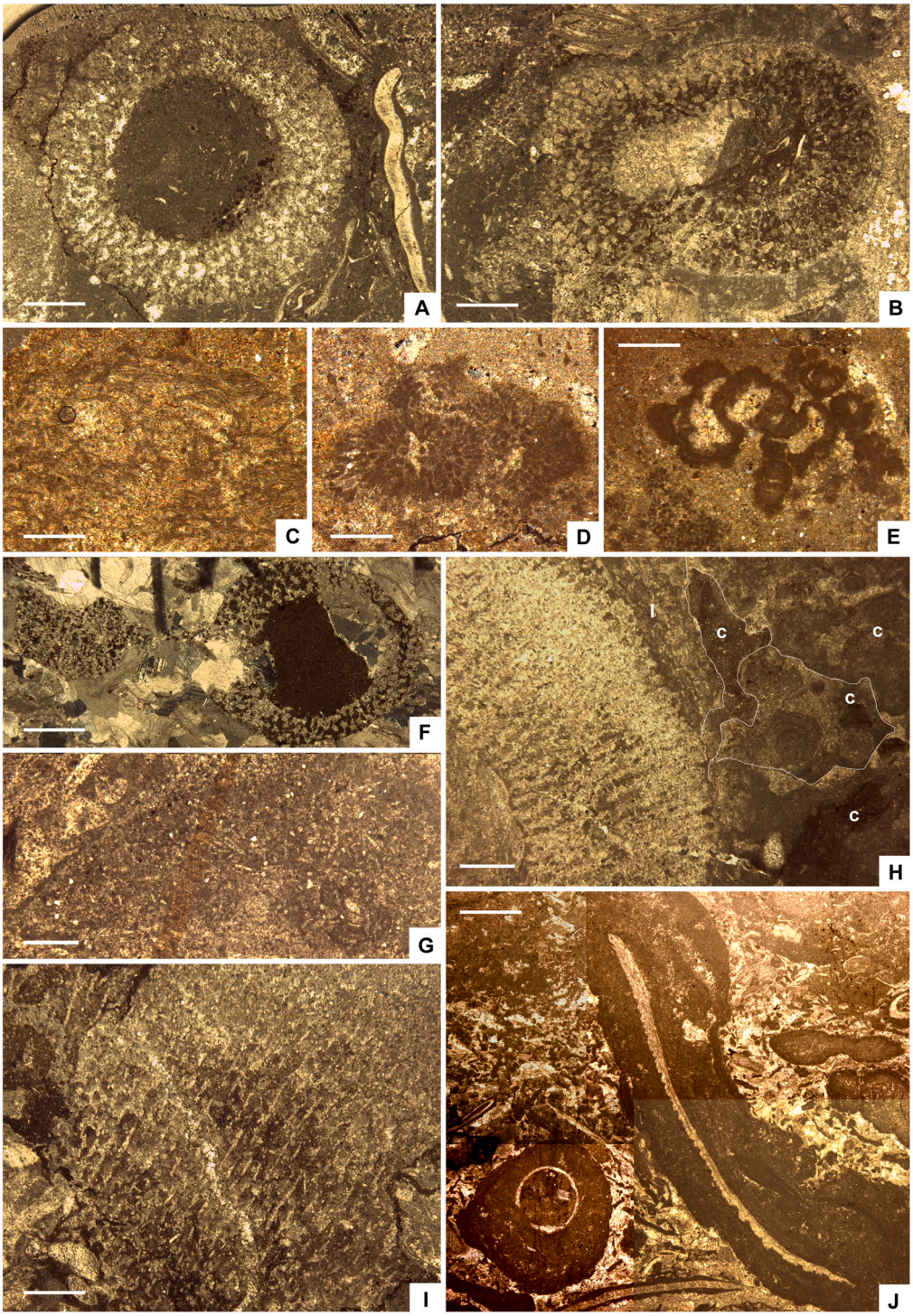


**Fig. 12.** Petrographic photomicrographs from the Shahmirzad anthaspidellid-microbial reef complexes and *Rankenella* debris from pelmatozoan-rhynchonelliformean accumulations. A. Transverse section of a *Rankenella* cup preserved in life position; level SH36 (stratigraphic setting in Fig. 3). B. Oblique section of *Rankenella* cup preserving a geopetal structure in the inner cavity; SH37. C. Subparallel filaments of *Girvanella* successively encrusting the muddy substrate in a section transverse to stratification; SH33. D. *Epiphyton* bush in a section parallel to stratification; SH33. E. *Renalcis* network with intraparticle pores infilled with mosaics of sparry calcite in a section parallel to stratification; SH32. F. Reworked debris of *Rankenella* cups with complete transverse section showing a geopetal structure with hematite cement, and fragmented (left) skeleton; Miaolingian pelmatozoan-rhynchonelliformean accumulation at Mila-Kuh stratotype; MK43. G. Detail showing infill of primary cavity by silty micrite (dermal surface on top-left); SH39. H. Outer wall of *Rankenella* encrusted by successive generations of laminated (l) and clotted (c) microbial textures displaying onlapping geometries; SH40. I. Longitudinal section of a *Rankenella* wall with ladder-like spiculate network; SH36. J. Irregular oncoids and pisoids of a patch-reef flank with cores composed of uncertain conical shell and rhynchonelliform valve; SH38. Scale bars = 2 cm (A–C, E–F, H) and 500 μm (D, G).

crusts, which episodically stabilized the shelly substrate, favouring development of thromboids and the cementation of their porous clots and interparticle pores. After development of such a complex intergrowth of thromboidal textures, anthaspidellid cones colonized the substrate, in some cases reaching 50 % in volume. Some sponges are simple cones, others are branching conical colonies, and some also display outgrowths fixed on other cones. Reef onlapping covers and flanks, composed of oncoidal rudstones and shelly packstones, thin away laterally, passing, over a distance of 1 to 2 m, into the typical shell beds generated by pelmatozoan-rhynchonelliformean meadows.

## 5. Firmground vs. hardground substrates

'Hard (carbonate) substrate' is a broad term that includes, among others, fossil and living, aragonite- and calcite-walled shells, beachrocks, rock-grounds (lithified substrates that have been exhumed) and partly to wholly, carbonate-cemented seafloor sediments (firmgrounds vs. hardgrounds; Rozhnov, 2001). By far, the most abundant biogenic hard substrates are provided by shell beds (Taylor and Wilson, 2003). In contrast, hardgrounds are 'synsedimentarily lithified carbonate seafloors that became hardened *in situ* by the precipitation of a carbonate cement in the primary pore spaces […] contemporaneously with or soon after deposition' (Wilson and Palmer, 1992: p. 3). Hardgrounds refer, therefore, to abiotic precipitation of calcite and would represent intervals of time 'soon after deposition' during which sedimentation did not take place and cement precipitated. Hardground development is not related to microbial growth. Firmgrounds, stiff but uncemented carbonate substrates, may be precursors of hardgrounds, and display intermediate consistency patterns that can be colonizable by both boring (hardground) and burrowing (softground) organisms. The problem is the distinction of the firmground/hardground boundary.

Although phosphate hardgrounds were relatively common since

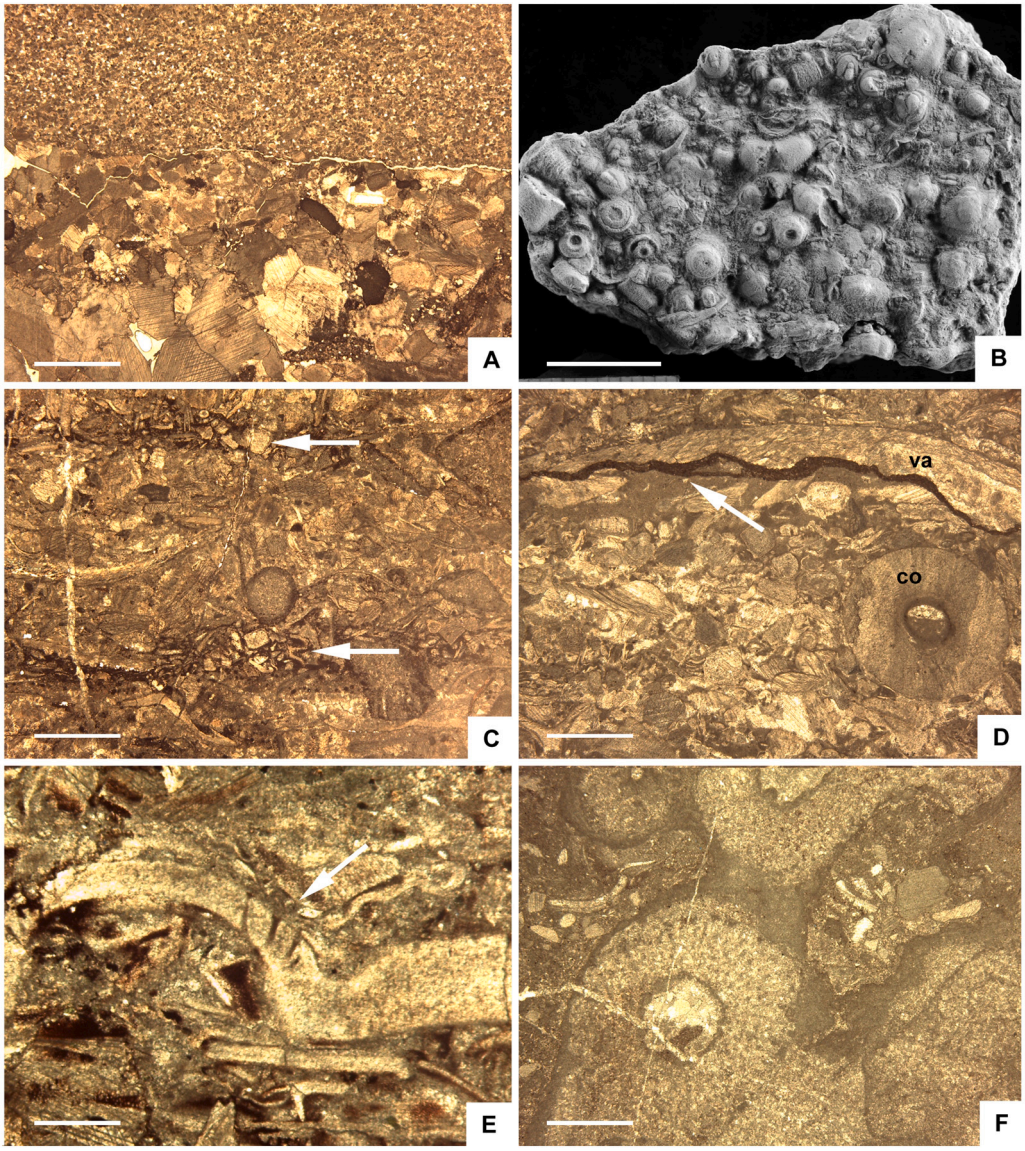


**Fig. 13.** Petrographic photomicrographs of hardgrounds, microboring textures and micritized skeletons from Members 2 and 3 of Mila Formation. A. Erosive contact of a lithified encrinitic packstone, behaving as a hardground, overlain by a siltstone; level MK23 (stratigraphic setting in Fig. 3) of Member 3. B. Lumachella with a mixture of agnostoid and trilobite cranidia, and bowl-shaped holdfast and columnal ossicles, whitened with ammonium chloride; ML26 in Member 2. C. Two subparallel porous interlaminae (arrowed) encrusted with iron oxyhydroxide; MK42 in Member 3. D. Packstone of monocrystalline and columnal (co) ossicles capped by a disarticulated rhynchonelliform valve (va) with shelter pore occluded with iron oxyhydroxide (arrowed); SH42 in Member 3. E. Trilobite sclerite showing straight and J-shaped (arrowed) microborings transverse to skeletal wall; SH42 in Member 3. F. Micritized walls of *Rankenella* cups displaying a broad muddy aspect, subsequently encrusted by several generations of thromboid crusts; SH38 in Member 3. Scale bars = 1 cm (A, C–D, F), 2 cm (B) and 500 μm (E).

Proterozoic times (e.g., Papineau, 2010), the earliest Phanerozoic carbonate hardgrounds are currently recognized from Miaolingian microbial-free carbonate strata of Argentine, Laurentia, Newfoundland and North China (Chow and James, 1992; Cowan and James, 1993; Srinivasan and Walker, 1993; Rankey et al., 1994; Oslager and Montañez, 1996; Brett et al., 2009; Gómez and Astini, 2015; Lee et al., 2015a; Peel, 2017) to Furongian strata of Iran (Rozhnov, 2001; Kruse and Zhuravlev, 2008), Laurentia (Brett et al., 1983; Chow and James, 1992; Cowan and James, 1993; Srinivasan and Walker, 1993; Sumrall et al., 1997) and North China (Chen et al., 2011; Lee et al., 2015b).

Shell pavements and shoals rich in echinoderm-brachiopod packstones-grainstones and rudstones, which characterize some distinct interbeds of Member 2 and the entire Member 3 of the Mila Formation, were irregularly subject to synsedimentary to earliest diagenetic precipitation of calcite and ferruginous cements on the seafloor to form hardground surfaces (see also Rozhnov, 2001; Kruse and Zhuravlev, 2008). They developed on truncated ooidal, oncoidal and peloidal wackestone-packestone (Fig. 13A) to grainstone, and flat pebble conglomerate. In some cases, the hardgrounds were subsequently encrusted by stromatolites and thrombolites and/or coated by iron oxyhydroxides (Fig. 13C–D), reflecting intervals of long exposure favouring calcite and iron oxyhydroxide precipitation. Their lithified character is supported by some scouring (erosive) tops separating them from overlying high-energy, sandy to silty shoals, as well as the record of encrusting holdfasts (Fig. 13B).

One of the oldest firmground to hardground transitions, based on the lateral gradation from mottled (burrowed) wackestone to packstone interbeds, encrusted by pelmatozoan holdfasts and cemented by early-diagenetic syntaxial overgrowths and occlusion of intraparticle skeletal and shelter porosity by mosaics of calcite, was reported from Miaolingian shelly carbonates of northern Spain and Morocco, western Gondwana (Zamora et al., 2010). Amphora- to bowl-like ossicles with proximally pierced holdfasts and longitudinally perforated nodal columnals, prolonged into a lobate to stellate crown of proximal appendages (diagnostic character of different parataxonomic species), are conspicuous skeletal elements of Furongian shelly debris in NE Spain (Álvaro and Colchen, 2002; Zamora et al., 2009), SW Sardinia (Loi et al., 1995), Norway (Erdtmann et al., 1984; Berg-Madsen, 1986) and the Alborz Mountains (Rozhnov, 2001: fig. 11.2) (see Fig. 13B). They developed anchoring strategies on clayey substrates and encrusting ones on carbonate substrates (Seilacher and MacClintock, 2005; Álvaro and Colchen, 2002). Similar late Miaolingian holomeric columnals encrusting hardgrounds have also been reported from Greenland (Peel, 2017). All these findings would support the distinct contribution of pelmatozoan ossicles to the occurrence and evolution of these early carbonate hardgrounds (Rozhnov, 2001), somewhat controlled by the stereom porosity network of these ossicles that certainly favoured the earliest diagenetic occlusion of intra- and interparticulate pores.

Early-diagenetic calcite cementation of mudstone and wackestone substrates, with their lower permeabilities, may be expected to take place much more slowly than those of highly permeable packstone and rudstone textures. In addition, aragonite tends to precipitate at higher supersaturation levels than calcite (calcite seas link to low-Mg calcite cements, $< 4$ mol% $MgCO_3$; Zhuravlev and Wood, 2008; Balthasar and Cusack, 2015) growing syntaxially on calcite hard substrates, such as those composed of echinoderm ossicles and rhynchonelliform valves. As a result, hardgrounds seem more common and faster growing in calcite than aragonite seas.

In the pelmatozoan-rhynchonelliformean shell beds and anthaspidellid-microbial reef complexes, surface-sediment micritization and subsequent degradation of carbonate allochems is represented by endolithic microboring (e.g., on trilobite sclerites, Fig. 13E). Micritic enveloping of echinoderm stereom pores and walls of *Rankenella* (Fig. 13F) is pervasive and related to synsedimentary microbial growth. Surface-sediment micritization was produced by microbial consortia, potentially dominated by (cyano-)bacteria with possible involvement of heterotrophic fungae, which persisted during sedimentary and early diagenetic timing. This contrasts with the microbial activity related to the photosynthetic (cyano-)bacterial activity linked to the formation of oncoids and mats.

## 6. Raman spectroscopic features of microbial textures

The ability of Raman spectroscopy to identify organic compounds and mineralogy at the microscale makes it particularly suitable for the study of microbial carbonates. Microbes can leave distinct structural and chemical signatures in carbonate minerals (organic remnants and mineralized microbial cells) that can thus be detected and mapped by Raman spectroscopy (e.g., Bower et al., 2013; Schito et al., 2019).

Two microbial textures from Member 3 of the Mila Formation were selected for Raman spectral analysis: micritized walls of *Rankenella* sponges (sample MK43 from Mila-Kuh) and oncoids (ML3 from Deh-Mola). The most prominent Raman signals in the lower wave-number region (Fig. 14A) are typical of amorphous carbon with peaks at ca. 1600 $cm^{-1}$ (graphite or G-band) and 1350 $cm^{-1}$ (disorder or D-band) (Quirico et al., 2009; Schito et al., 2022). Peak intensities of both bands can vary in a small range due to thermal alteration, carbon crystallinity (both parameters similar for all the analyzed material) and the original carbonaceous material (Marshall et al., 2010). The D-band is related to the presence of in-plane defects and heteroatoms (Beny-Bassez and Rouzaud, 1985), whereas the G-band is indicative of an increase in graphitic crystalline order (Bower et al., 2013). In the Alborz samples, the D-band is split into the D1-band (~1350 $cm^{-1}$), D4-band (~1250 $cm^{-1}$) and D3-band (~1500 $cm^{-1}$) (Fig. 14B), which suggest structural defects (Beny-Bassez and Rouzaud, 1985), and are visible after the Lorentzian deconvolution of the former peaks. The D2-band, which usually appears around 1620 $cm^{-1}$, has not been identified due to the low diagenetic grade of the samples, as a result of which, the separation of the G and D2 bands is unavailable, resulting in a single band located around 1600 $cm^{-1}$ (Beyssac et al., 2002). Both samples show a morphology characteristic of poorly organized organic matter, reminiscent of the low-grade samples of the Glaurus Alps studied by Lahfid et al. (2010). The D-band is wide and less intense than the G-band, with a noticeable shoulder caused by the D4 band in the MK_43 sample. The intensity and position of the D4-band increases in an inverse relationship with the metamorphic grade, disappearing once perfect graphitic order is reached (Lahfid et al., 2010). The G-band is narrow and, as previously mentioned, probably contains both the G-band and the D2-band (Beyssac et al., 2002).

Following Bower et al. (2013) and Luo et al. (2014), among others, two parameters were selected for taphonomic comparison of carbonaceous material, with compositionally different precursor material, and low diagenetic thermal affection: $\Gamma_D$ (full width at half height of D-band) and R1 (intensity ratio of D- and the G-band). The calculations of the intensity ratio R1 values (Wopenka and Pasteris, 1993) below 1, for both samples, suggest a low diagenetic/metamorphic grade, with MK_43 having a lower R1 ($0.53 \pm 0.029$) than ML_3 ($0.69 \pm 0.014$). $\Gamma_D$ values range from $160.67 \pm 4.37$ $cm^{-1}$ in MK_43 to $170 \pm 4.78$ $cm^{-1}$ in ML_3. When plotting the average $\Gamma_D$ vs R1 values, both carbon signals are clearly different. As both signals are preserved under similar burial and thermal diagenetic conditions, both clusters support different precursor (microbial) material (Luo et al., 2014).

The distinct association of organic material in laminated oncoids/pisoids and bioerosive textures affecting micritized walls of *Rankenella* sponges suggests different microbial consortia in the record of framebuilding (constructive activity) microbial laminae and microboring (bioerosive or destructive factor) textures.

## 7. Tectonic control on carbonate productivity and reefal development

The early Palaeozoic infill of the Alborz basin fringing northeastern

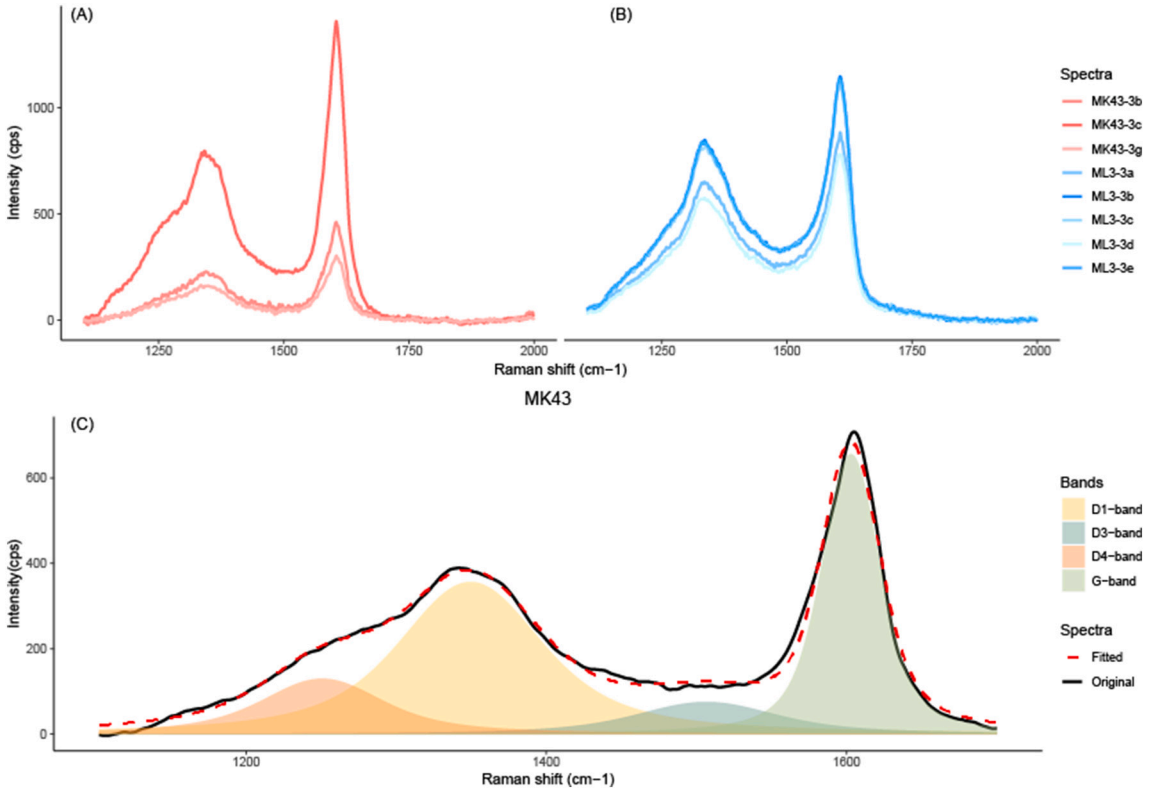


**Fig. 14.** Representative Raman spectra of organic matter remains from Member 3 of Mila Formation, at room temperature. A. Spectra from micritized *Rankenella* walls (level MK43 in Mila-Kuh). B. Spectra from an oncoid cortex (level ML3 in Deh-Mola). C. Deconvolution framework by fitting to a four-band Lorentzian profile, performed by Peak Resolve (OMNIC from Termo Fischer Software), of former *Rankenella* wall, marked by individual local vibrational modes; deconvoluted peak positions at 1250.704 $cm^{-1}$ (D4), 1349.580 $cm^{-1}$ (D1), 1506.426 $cm^{-1}$ (D3), and 1602.911 $cm^{-1}$ (G).

Gondwana recorded the progradation of quartz-rich siliciclastic blankets, which derived from widespread denudation of the Arabian-northeastern African basement (Horton et al., 2008; Zoleikhaei et al., 2021, and references therein). However, the sandy shoal complexes were episodically interrupted, during Cambrian Epoch 2 to Furongian times, by nucleation of microbial and shelly carbonate factories. As documented by synsedimentary extensional tectonics laterally linked to both major scouring surfaces (interpreted as unconformities) and olistostrome and slope-related aprons, selected for subdividing lithostratigraphically the Mila Formation, the Gondwana margin locally recorded sharp modifications in accommodation space controlled by extensional pulses (Álvaro et al., 2022), which regulated reefal growth.

The Cambrian Series 2 to Lower Ordovician lithostratigraphic units of the eastern Alborz Mountains are commonly bounded by unconformities: (i) the Lalun/Fasham contact represents a palaeorelief inherited from the incision of tidal shoal complexes (Bayet-Goll et al., 2018, 2021) (Fig. 15A); (ii) the Fasham/Member 1 contact is marked by an ironstone crust rich in hematite and hematitic clayey matrix, which has been interpreted by Lasemi and Amin-Rasouli (2016) as a paleosol; (iii) the Mila 1/Mila 2 contact is characterized at the Mila-Kuh stratotype by a distinct erosive scar capped by mass transport events (e.g., olistoliths and olistostromes, about 20 m thick, involving dolostone

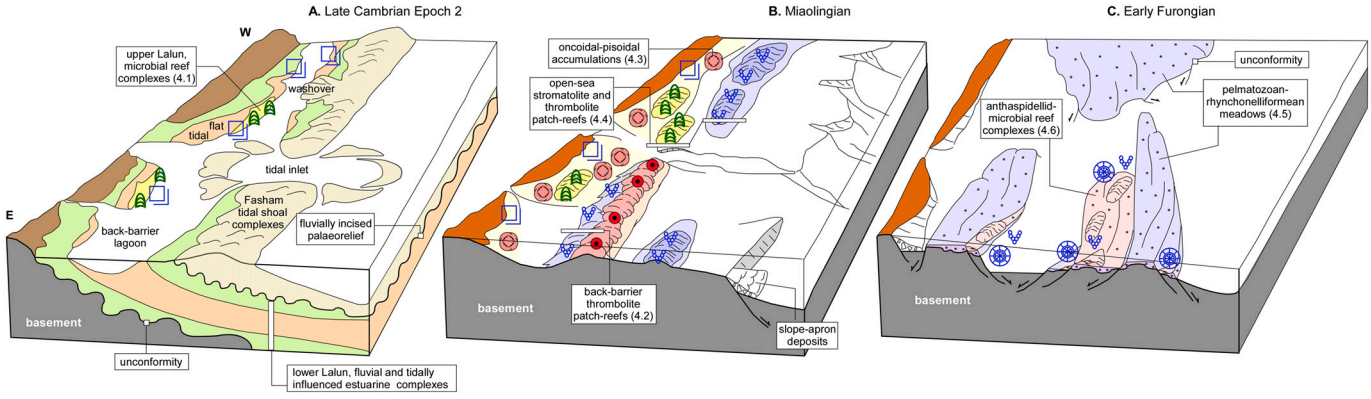


**Fig. 15.** Tentative palaeogeographic reconstruction of the Alborz Basin fringing the northeastern Gondwana margin, during Cambrian Epoch 2 to Furongian times. A. Late Cambrian Epoch 2 barrier-lagoon system with development of microbial (stromatolitic) reef complexes; upper member of the Lalun Formation. B. Miaolingian back-barrier/shoal environments with setting of protected oncoidal-pisoidal accumulations and thromboid patch-reefs, and lateral open-sea microbial (thromboid and stromatoid) patch-reefs; Members 1 and 2 of Mila Formation. C. Early Furongian horst-and-graben palaeotopography with setting of pelmatozoan-rhynchonelliformean meadows and thickets, and anthaspidellid-microbial reef complexes; Member 3 of Mila Formation. Not to scale.

packages sourced from Member 1; Álvaro et al., 2022: fig. 7c–d) (Fig. 15B); (iv) the Mila 2/Mila 3 contact exhibits a distinct erosive surface, with incisions up to 8 m deep at Deh-Molla, associated with penecontemporaneous normal faults (Shahmirzad and Deh-Sufian logs; Álvaro et al., 2022: figs. 7g–h, 8c–d) and the apparent gap of a trilobite zone (Peng et al., 1999) (Fig. 15C); and (v) the strata of the Mila 3, 4 or 5 members can be unconformably overlain by the Sime-Kuh Formation, implying the whole denudation of Furongian strata; at Mila-Kuh log, the unconformity follows a palaeorelief, mimicking synsedimentary grabens affecting Members 3 to 5, and subsequently sealed by the Simeh-Kuh shales (Álvaro et al., 2022: fig. 8b). Another striking control of tectonic activity is emphasized by the record of the above-reported anthaspidellid-microbial reef complexes at Shahmirzad, so far reported from hanging-wall blocks.

As a result, the Cambrian Series 3 to Lower Ordovician strata cropping out throughout the central and eastern Alborz Mountains do not

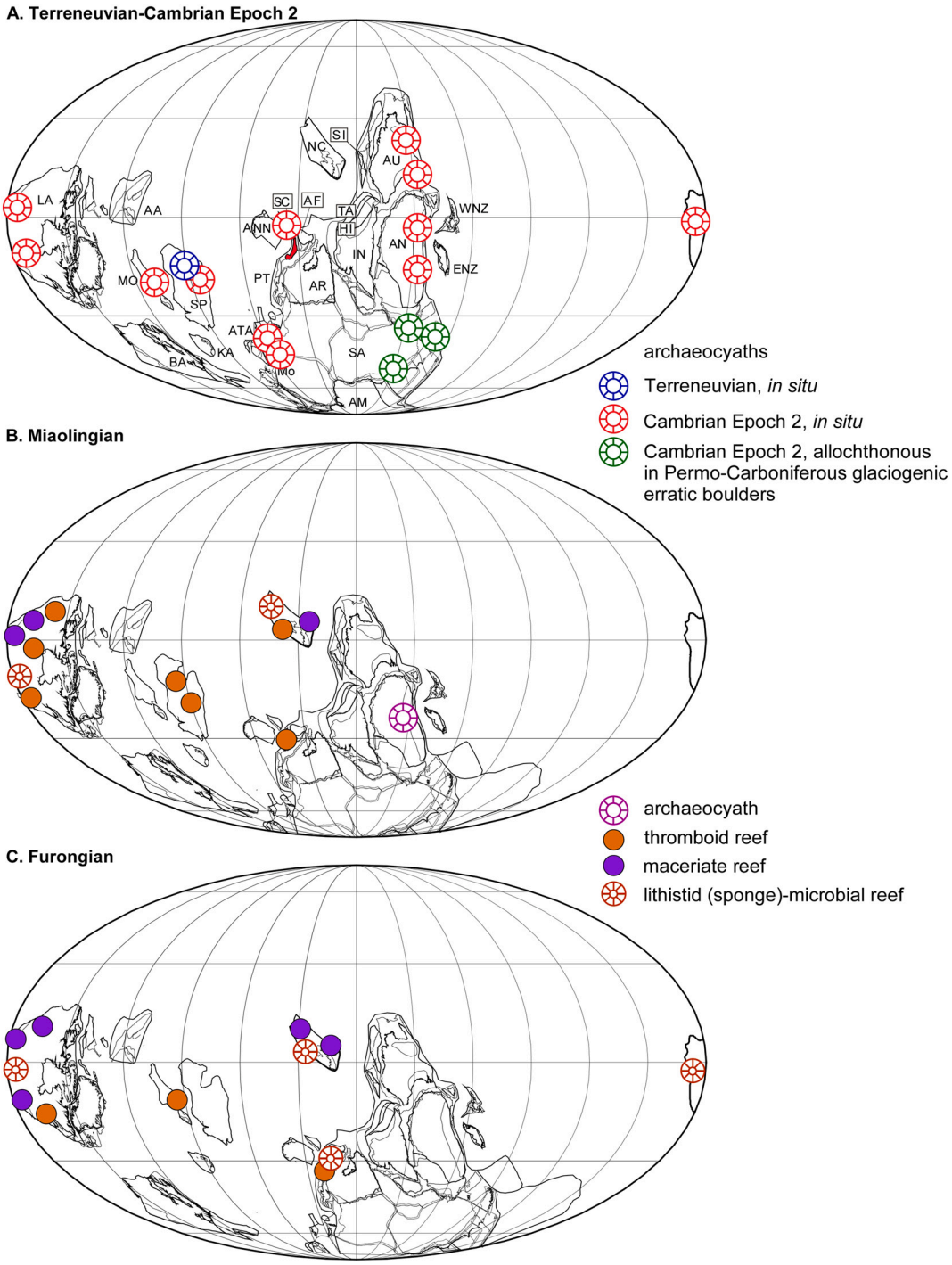


**Fig. 16.** Global palaeogeographic occurrence of Cambrian metazoan-microbial reef complexes based on references cited in the text; reconstruction modified from Álvaro et al. (2013b). A. Terreneuvian–Cambrian Epoch 2. B. Miaolingian. C. Furongian. Abbreviations: AA Arctic Alaska-Chukotks, AF Afghanistan, Am Amazonia, AN Antarctica, ANN Annamia, AR Arabia, ATA Armorican Terrane, AU Australia, BA Baltica, ENZ Eastern New Zealand, KA Kara Terrane, LA Laurentia, MO Mongolia, Mo Morocco, NC North China (Sino-Korean Block), Pt Pontides-Taurides, SA South America, SC South China (Yangtze Block), SI Sibumasu, SP Siberian Platform, WNZ West New Zealand.

represent a stable ramp, but a fault-block carbonate platform with (i) a land area to the (present-day) south linked to the northern Turkish-Iranian-Afghan margin of Gondwana; and (ii) a narrow seaway separating the margin from South China and allowing close biogeographic connections (Álvaro et al., 2013b; Ghobadi Pour et al., 2022). This Gondwana margin recorded stepwise sharp modifications in accommodation space controlled by extensional pulses that have been linked to rifting conditions (Álvaro et al., 2022).

Finally, drowning of such a framework of tilted platform-blocks at the Mila 3/Mila 4 transition required a change in the environmental regime, such as (i) a rapid short-term transgression across the Furongian–Tremadocian transition; (ii) a significant increase in terrigenous input, dramatically affecting carbonate factories, as a combination of eutrophication (from nutrient influx) and physical burial by high sedimentation rates (see Li et al., 2021); (iii) a major pulse of tectonic subsidence, or (iv) a combination of these processes (see similar mechanisms in Masse and Fenerci-Masse, 2013; Brandano et al., 2015; Betzler et al., 2023).

## 8. Global evolution of Miaolingian–Furongian reef complexes

### 8.1. Extinction crisis across the Cambrian Epoch 2–Miaolingian transition

Debrenne (1991), Kruse et al. (1995) and Rowland and Shapiro (2002), among others, had proposed the Siberian Platform as the late Cambrian Age 2 biogeographic origin of archaeocyaths, from where they migrated worldwide. However, Wang et al. (2025) have recently reported the record of Fortunian microscopic archaeocyaths in South China, supporting their biomineralization in the beginning of the Cambrian explosion. This taxon represents the leading metazoan participant of the Cambrian Epoch 2 microbial-dominant reefs. Archaeocyaths were aspiculate hypercalcified sponges which colonized both soft muds and substrates formerly encrusted by microbial communities, mainly related to the calcimicrobes *Epiphyton*, *Girvanella* and *Renalcis*. They locally occur associated with other subsidiary frame-building metazoans, such as coralomorphs, cribicyaths and radiocyaths (Kruse et al., 1996; Wood, 1999; Pratt et al., 2001; Hicks, 2006). Archaeocyathan-microbial reefs also incorporated calcarean (with calcareous spicules) and silicean (demosponge and hexactinellid) spicules (Debrenne and Reitner, 2001), e.g. hexactinellid (siliceous) spicules occur in reefal cores and flanks in Siberia (Dzik, 1994; Kruse et al., 1995) and the Australian Flinders Ranges (James and Gravestock, 1990; Brunton and Dixon, 1994; Reitner and Mehl, 1995).

The Fortunian occurrence of archaeocyaths pre-dated that of trilobites, and reached their diversity peak across the Age 3–4 boundary interval (Cambrian Epoch 2; Zhuravlev and Naimark, 2005) (Fig. 16A). A two-phase extinction event took place in the end of Cambrian Epoch 2 triggering the virtual demise of the archaeocyaths and the related collapse of metazoan-bearing reefs. In the Siberian Platform, Zhuravlev (1996) reported a mid–Botoman generalized anoxia owing to eutrophication, and an early–Toyonian worldwide regression (Hawke Bay event and lateral equivalents). Zhuravlev et al. (2022) correlated an oxic pulse at about 521–519 Ma with reefal expansion associated with a gradual increase in average reef size and complexity. The interval of expanded marine anoxia (about 519–516.5 Ma) led to reefal and archaeocyathan body size reduction and coeval increased rates of extinction. A succeeding oxic pulse at ca. 515 Ma led to renewed expansion of reefal communities, and increased archaeocyathan body size and diversity, but linked to weaker community-wide environmental responses (Zhuravlev et al., 2023).

After these anoxic episodes, late-Age 4 archaeocyaths persisted as a 'dead clade walking' (*sensu* Pruss et al., 2024) in Mid–Toyonian assemblages of South China (*Archaeocyathus yanjiaoensis*; Yang et al., 2016), Australia (*A. abacus*; Kruse, 1991), and northern Spain (*A. laqueus*, *Pycnoidocyathus erbiensis*, *Okulitchicyathus valdorensis* and *Polythalamia* sp., probably in need of taxonomic revision; Perejón and Moreno-Eiris, 2003). These last archaeocyaths displayed a dramatically low diversity (Debrenne et al., 2015). Finally, putative archaeocyaths have been reported from the Miaolingian of Antarctica (Wood et al., 1992).

Although archaeocyaths commonly played a subordinate role in reef building, and took advantage of the stabilization of soft substrates induced by microbially induced encrustation (Wood et al., 1992; Debrenne and Reitner, 2001), some pioneer archaeocyaths were able to colonize clayey (soft) substrates becoming the first settlers providing the substrate for calcimicrobes (Wood et al., 1993; Kruse et al., 1995; Riding and Zhuravlev, 1995). Thromboid textures and synsedimentary to earliest diagenetic cementation fulfilled the main frame-building role (Pratt et al., 2001; Álvaro et al., 2006). Their adaptability was somewhat constrained: in the morphological disparity analysis of Laurentian archaeocyaths carried out by Cordie and Dornbos (2019), two major constraints were recognized: (i) an average cup/individual (body) diameter of 10.6 mm, significantly smaller than any modern demosponge (including lithistids), and (iii) their reduction to a few simple morphologies. Archaeocyaths were, therefore, restricted in their morphological complexity, representing a dramatic limitation to adaptation and potentially representing an increased risk of extinction under sharp environmental modifications.

### 8.2. Miaolingian–Furongian recovery

The collapse of archaeocyathan communities broadly coincided with new evolutionary adaptations of spiculate sponges and pelmatozoan echinoderms, which progressively became primary metazoan contributors to Miaolingian non-reefal and Furongian reefal communities (Fig. 16B). The structure of Terreneuvian–Cambrian Epoch 2 spiculate sponges was relatively simple: monaxonids and hexactinellids developed thin-walled conical morphs with single layers supported by spiculate networks (Carrera and Botting, 2008). Elongated, cup to palmate-shaped forms mainly occupied passive suspension-feeding niches in quiet-water substrates (Finks, 2003a, 2003b). However, complex skeletons occurred across the Cambrian Epoch 2–Miaolingian transition. They exhibited intricate channels and cavities that favoured the passage of water and minimized the damaging effects of agitated waters and strong currents. As a result, some spiculate sponges increased their active pumping capabilities, refining their own currents through choanocyte-flagellar movement (Leys et al., 2011; Botting and Muir, 2018) and developing an active control over the volume of water they processed (Ludeman et al., 2017). This adaptation allowed them to exploit more dispersed food resources as efficient filter feeders in shallow-water environments. This strategy was shared by brachiopods, which were able to generate their own current through their lophophore structure (Williams et al., 2002), and pelmatozoans (Zamora et al., 2010). A microbial mat/pelmatozoan antagonistic relationship has been claimed based on the non-overlapping palaeogeographic distributions of Cambrian Epoch 2 pelmatozoans *versus* microbial reefs and mats (Álvaro et al., 2013a).

Mid-latitude settings, dominated by mixed (siliciclastic-carbonate) substrates, recorded the widespread development of chancelloriid-echinoderm-spiculate sponge (CES) meadows (Álvaro and Vennin, 1997; Álvaro et al., 2013a). Their skeletal debris globally covered the seafloor leading to the occurrence of porous shelly substrates that, submitted to earliest diagenetic calcite cementation, locally became firmgrounds to hardgrounds (Zamora et al., 2010; Álvaro and Mills, 2024).

The occurrence of thicker-walled and more robust spiculate sponges is highlighted by the record of the first (wholly articulated) lithistid sponges. They constitute a long-ranging polyphyletic group of demosponges (Morrow and Cárdenas, 2015; Schuster et al., 2015) that persist at present (Maldonado et al., 2015). Externally, anthaspidellids broadly resemble archaeocyath non-spiculate sponges, with which they also share their reef-building role (Hong et al., 2016; Lee et al., 2016a). All

Cambrian lithistid sponges so far belong to the Family Anthaspidellidae, which share a conical morphology and a distinctive ladder-like spiculate structure. The earliest known lithistid is *Rankenella*, which occurred near the Age 4/5 boundary (Kruse, 1996). Their first complete skeletons appeared in the Miaolingian of Australia, Laurentia and North China (Dattilo et al., 2004; Mrozek et al., 2003; Shapiro and Rigby, 2004; Kruse and Reitner, 2014; Lee et al., 2016b), but the taxon became abundant in the Furongian, mainly due to their 3D preservation in reefal cores (Fig. 16B). Orchocladine demosponges, in particular the anthaspidellids, developed thicker walls, which led to the occurrence of interlocking spicules in sturdy, ladder-like, desma-based, triangulated nets (Finks, 2003a). Cemented attachments, allowed them to occupy shallower environments, including reef settings under agitated waters (Kruse and Reitner, 2014).

Furongian frame-building anthaspidellid sponges include *Rankenella mors* (late Drumian, Australia; Kruse and Reitner, 2014), *R. hamdii* (early Paibian, Iran; Hamdi et al., 1995; Kruse and Zhuravlev, 2008), *R. zhangxianensis* (latest Age 5 to early Guzhangian, North China; Lee et al., 2016a), *Gallatinospongia conica* (early Paibian, Nevada and California; Shapiro and Rigby, 2004), *Wilbernicyathus donegani* (Jiangshanian–Stage 10, Texas and Colorado; Johns et al., 2007), and an unidentified anthaspidellid sponge (Jiangshanian–Stage 10, Nevada, Mrozek et al., 2003; Dattilo et al., 2004) (Fig. 16C). These sponge-bearing reefs were encrusted by microbial consortia (e.g., *Epiphyton*, *Girvanella*, *Renalcis*, and *Tarthinia*). Hexactinellids and some non-lithistid demosponges also began to colonize shallow-water non-reefal environments (Botting and Muir, 2018). Throughout the Miaolingian and Furongian, a time span of ca. 25 m.y., metazoan reefs mainly consisted of microbial carbonates associated with conical lithistid sponges. Other minor Miaolingian to Furongian reefal metazoans include coralomorphs (e.g., *Cothonian* and *Lipopora* in Age 4, and *Tretocylichne* in Age 5; Park et al., 2016), a possible cnidarian from late Age 5/early Drumian (*Cambroctoconus*; Park et al., 2011), and a possible recumbent ceroid to phaceloid coral (*Cambrotrypa* in the Miaolingian; Scrutton, 1997).

Lithistid-microbial reefs also shared their frame-building niches with maceriate sponge-microbial reefs. The latter consist of centimetre-scale maceria structures, which developed branching, domal, columnar and digitate shapes in longitudinal section (Shapiro and Awramik, 2006; Lee et al., 2010). According to the macerial composition and the intermacerial sediment, these reefs are subdivided into muddy, grainy and dolomitized maceriate reefs. Muddy and grainy maceriate reefs contain siliceous sponge spicule networks and thromboid components, such as *Girvanella* and rare *Tarthinia* (Lee et al., 2014). The maceria structures would reflect, as a result, symbiotic-like frame-building frameworks composed of siliceous sponges, microstromatolites and thromboid textures. The broad lack of detrital carbonate within maceriae textures indicates that binding and trapping processes by microbes and sponges were subsidiary controls (Chen et al., 2014).

It is remarkable how the strong biogeographic similarities displayed by the Miaolingian to Ordovician trilobite, brachiopod and conodont assemblages of the Alborz Mountains and the neighbouring South China Block (Peng et al., 1999; Álvaro et al., 2013b, 2022; Popov et al., 2013; Geyer et al., 2014; Jahangir et al., 2016; Holmer et al., 2019) are not shared by their frame-building structures. Maceriate sponge-microbial reefs, with maceria structures of siliceous spiculate networks, are abundant in the Sino-Korean microcontinent (South China), Laurentia, Siberia and Australia (Shapiro and Rigby, 2004; Hong et al., 2012, 2016; Chen et al., 2014; Lee et al., 2014, 2015b, 2016a, 2019, 2021; Adachi et al., 2015; Xiao et al., 2018), whereas lithistid (anthaspidellid)-microbial reefs, similar to those reported in the Alborz Mountains (Hamdi et al., 1995; Kruse and Zhuravlev, 2008), have been so far exclusively reported in SW Laurentia (Mrozek et al., 2003; Dattilo et al., 2004; Shapiro and Rigby, 2004; Johns et al., 2007; Lee et al., 2016b), Australia (Kruse and Reitner, 2014) and North China (Lee et al., 2016a).

### 8.3. Abiotic factors

In the absence of direct competitors for reef-building and reef-dwelling niches, which appeared in the Furongian (Lee et al., 2019; Cordie, 2023), abiotic factors seem to be more significant drivers for the extinction of archaeocyaths. Debrenne (1991) invoked drift into cooler latitudes for many palaeocontinents and the consequent foundering of carbonate platforms. However, based on the Cambrian counter-clockwise rotation of Gondwana, this argument may be only applied to its western margin (e.g., Morocco and SW Europe), where carbonate production was residual during the Miaolingian and Furongian.

Several databases related to carbonate and reefal preservation throughout Cambrian times provide further information, although their quality depends on the range of their analyzed chronological intervals. A database of the estimated extent in $km^2$ of Phanerozoic carbonate platforms (Smith et al., 2021) shows a distinct fall from Cambrian Epoch 2 to Miaolingian–Furongian times. This trend contrasts with the progressive increase in the carbonate relative abundance across the same time span preserved in sedimentary rocks from Laurentia (Wang et al., 2023). These opposing trends reflect a drastic fall in Miaolingian–Furongian carbonates in continents other than Laurentia, which is also reflected by the coeval fall in the preservation of worldwide reef volume (Raja et al., 2023). The lack of Furongian strata was, for instance, one of the consequences related to the record of the break-up (or rift-drift) unconformity throughout the Atlas – Ossa-Morena – Northarmorican Rift along West Gondwana, which led to generalized subaerial exposure, erosion and denudation of its Miaolingian basement (Álvaro et al., 2024).

The widespread development of hardgrounds by the late Miaolingian may be considered as controlled by the interplay of, at least, three factors: (i) the increase in abundance, thickness and size of available low-Mg calcite skeletons promoting the appearance of relatively resistant calcareous grainy substrates (Droser and Li, 2001); (ii) an increase in the global wealth of pelmatozoan meadows that favoured substrate stability by earliest diagenetic cementation, like in the case of the Mila 3 Member, rich in centimetre- to decimetre-thick shell beds composed of large low-Mg calcite rhynchonelliformean brachiopod valves; and (iii) greenhouse conditions linked to rapid marine cementation, and replacement of aragonite marine cements by calcite.

Several hypotheses have been proposed to explain the Miaolingian–Furongian scarcity of metazoan reefs, which led to a relative increase in the abundance of microbial reefs (Kiessling et al., 2002; Riding and Liang, 2005). A drastic change in $CO_2$ and nutrient availability would have been worldwide triggered by the eruption of the Kalkarindji flood basalts on northern Australia (eastern Gondwana; Glass and Phillips, 2006; Hough et al., 2006; Myrow et al., 2024). Rowland and Shapiro (2002) invoked a combination of nutrient shortage, high levels of atmospheric $CO_2$ (potentially linked to oceanic acidification; Kiessling and Simpson, 2011), seawater Mg/Ca chemistry, and global warming. The latest Cambrian Epoch 2 Hawke Bay–Toyonian Regression necessarily affected the availability of shallow epeiric seas (the main target for archaeocyathan-microbial nucleation). Global regressive conditions broadly persisted during the Miaolingian and Furongian (van der Meer et al., 2022, 2025), which coincided with relative low values in $O_2$ percentage (Berner, 2006). The Cambrian Epoch 2–Miaolingian transition also coincided with a significant turnover in skeletal biomineralization, replacing dominant high-Mg calcite and aragonite shells (aragonite seas with $m$Mg/Ca > 2 and low $pCO_2$) to low-Mg calcite skeletons (calcite seas with $m$Mg/Ca < 2 and high $pCO_2$; Zhuravlev and Wood, 2008; Wood and Zhuravlev, 2012). Low-Mg calcite skeletons appear to become advantageous in Miaolingian times, severely affecting the survival of massive poriferan skeletons of aragonite or high-Mg calcite minerals. In contrast, evidence for primary aragonite/high-Mg calcite persisting in the Furongian has been locally suggested by Neilson et al. (2016).

In summary, the trend to reduced diversity patterns of archaeocyaths

toward the late Cambrian Epoch 2, and disappearance thereafter, seems compatible with the coeval aragonite to calcite turnover in skeletal mineralization. This trend broadly coincided with a progressive lowering of the oceanic Mg/Ca ratio (probably related to the interplay of mid-ocean ridge volume and seafloor spreading rates of mid-ocean ridges; e.g., Sandberg, 1983; Stanley and Hardie, 1998; Rowland and Shapiro, 2002; McKenzie et al., 2014), dramatically punctuated by a global (Toyonian) regression. The Miaolingian–Furongian represents a prolonged interval of 'greenhouse' conditions, characterized by (i) a distinct Furongian fall in $^{87}Sr/^{86}Sr$ ratios and $\varepsilon_{toc}$ (isotopic fractionation between total organic carbon and sedimentary carbonates), from 493 to 444 Ma, linked to a distinct increase in atmospheric and oceanic $pCO_2$ (Rothman, 2002; Berner, 2009; Peters and Gaines, 2012; McKenzie et al., 2014; Chen et al., 2022; Bednarick et al., 2024); punctuated by (ii) the SPICE, taking place at ca. 497 Ma and lasting about 2 m.y., which has been linked to a rise in atmospheric $O_2$ that increased nutrient abundance, plankton diversity and development of localized oceanic anoxic conditions (Gill et al., 2011; Saltzman et al., 2011, 2015). The potential role of flourishing photosynthetic microbial factories in oxygenating shallow waters, even if broader abiotic conditions were less favourable, should also be taken into consideration (Li et al., 2024). Lee and Riding (2018) proposed that these elevated temperatures would have favoured lowered oxygen solubility, promoting extensive thermal stratification supporting marine disoxia and hypoxia, limiting the development of many metazoan reef-builders. The same authors proposed that lithistid sponges were somewhat predisposed to tolerate low oxygen levels, which would represent a key factor in their Miaolingian–Furongian success as reefal frame-builders. However, the first anthaspidellid debris of the Alborz Mountains occur reworked within the late Miaolingian pelmatozoan-rhynchonelliformean, low-angle shoal accumulations, induced by wave and storm currents and deposited under well-oxygenated conditions (Fig. 12C), which comprise the *Nisusia* Biofacies (Holmer et al., 2019). The same anthaspidellid taxa, associated with thromboid textures, developed frame-building fabrics in similar Furongian shallow-water bioaccumulations (Billingsellid Biofacies; Popov et al., 2011, 2013), directly controlled by tectonic activity, due to their exclusive nucleation and growth on tilted hanging-wall blocks in the vicinity of Shahmirzad town.

## 9. Conclusions

Despite the traditional paradigm that considers the growth of metazoan-bearing reefs was inhibited during the Miaolingian–Furongian interval, this overall decline should be seen in a global perspective taking into account the fall in the global volume of preserved carbonates and reefs. The Alborz margin that fringed Northeast Gondwana during the same time span displays a significant contrast, due to its pene-contemporaneous increase in microbial and shelly carbonate productivity, mainly controlled by a diverse and abundant shelly fauna (pelmatozoans and rhynchonelliformean brachiopods) which played a key role in the modification of grainy substrates. These evolved to highly porous shelly accumulations, which favoured the development of hardgrounds and, in hanging-wall blocks episodically protected from persistent wave and storm action, led to the nucleation and growth of anthaspidellid-microbial reef complexes. The first anthaspidellid debris of *Rankenella* occurred in similar late Miaolingian substrates (the first occurrence of the genus is indeed from near the Age 4/5 boundary in Australia), but the first frame-building skills of this genus were controlled in the Alborz margin by tectonic activity and substrate (firm- to hardground) properties.

Despite the worldwide occurrence of potential frame-building taxa in the Miaolingian, their capacity for participating in reefal fabrics does not seem to be controlled by a single factor but a combination of several interplaying ones, such as the modification in the oceanic Mg/Ca ratio controlling biomineralization, and the gradual increase in atmospheric and oceanic $pCO_2$, linked to nutrient abundance and development of localized oceanic anoxic conditions. However, disoxia and hypoxia conditions are seemingly absent in the Alborz margin of northeastern Gondwana, where the Miaolingian immigration of the anthaspidellid *Rankenella* from the Australian eastern margin of Gondwana favoured their subsequent Furongian success as a metazoan reefal key player.

## CRediT authorship contribution statement

**J. Javier Álvaro:** Writing – review & editing, Writing – original draft, Validation, Supervision, Methodology, Investigation, Funding acquisition, Formal analysis, Conceptualization. **Aram Bayet-Goll:** Writing – review & editing, Validation, Supervision, Investigation. **Mehdi Daraei:** Writing – review & editing, Visualization, Validation, Supervision, Investigation. **Blanca Martínez-Benítez:** Writing – review & editing, Visualization, Validation, Supervision, Methodology, Investigation.

## Declaration of competing interest

The authors declare that they have no known competing financial interests or personal relationships that could have appeared to influence the work reported in this paper.

## Acknowledgements

We appreciate the constructive and useful revisions made by Amalia Spina and two anonymous reviewers, and the suggestions by editor-in-chief (Catherine Chagué). JJA acknowledges with gratitude the support received in the field from Mansoureh Ghobadi Pour, Mohammad-Reza Kebria-ee Zadeh, Vachik Hairapetian and Leonid E. Popov. JJA and BMB warmly thank Ioanna Theodorou and Laura Tormo from MNCN by technical assistance. Research was funded by IGEO-IASBS scientific collaboration agreement and project PID2021-125585NB-I00 from the Spanish Ministerio de Ciencia, Innovación y Universidades and Agencia Estatal de Investigación.

## Data availability

No data was used for the research described in the article.

## References

Abbassi, N., Hadi, M., 2023. Ichno-biodiversity of Mila Formation in Cambrian–Ordovician interval north Shahmirzad section, Central Alborz. Stratigraphy and Paleontology 1, 60–69.
Adachi, N., Ezaki, Y., Liu, J., 2011. The oldest bryozoan reefs: a unique Early Ordovician skeletal framework construction. Lethaia 45, 14–23.
Adachi, N., Kotani, A., Ezaki, Y., Liu, J., 2015. Cambrian series 3 lithistid sponge-microbial reefs in Shandong Province, North China: reef development after the disappearance of archaeocyaths. Lethaia 48, 405–416.
Álvaro, J.J., Clausen, S., 2006. Microbial crusts as indicators of stratigraphic diastems in the Cambrian Brèche à *Micmacca*, Atlas Mountains of Morocco. Sedimentary Geology 185, 255–265.
Álvaro, J.J., Colchen, M., 2002. Earliest Ordovician pelmatozoan holdfasts from western Europe: the *Oryctoconus* problem revisited. Eclogae Geologicae Helvetiae 95, 451–459.
Álvaro, J.J., Debrenne, F., 2010. The Great Atlasian Reef Complex: an early Cambrian subtropical fringing belt that bordered West Gondwana. Palaeogeography, Palaeoclimatology, Palaeoecology 294, 120–132.
Álvaro, J.J., Mills, A., 2024. Carbonate production and reef building under ferruginous seawater conditions in the Cambrian rift branches of the Avalon Zone, Newfoundland. Sedimentology 71, 1245–1269.
Álvaro, J.J., Vennin, E., 1997. Episodic development of Cambrian eocrinoid-sponge meadows in the Iberian Chains (NE Spain). Facies 37, 49–64.
Álvaro, J.J., Vennin, E., 1998. Stratigraphic signature of a terminal Early Cambrian regressive event in the Iberian Peninsula. Canadian Journal of Earth Sciences 35, 402–411.
Álvaro, J.J., Clausen, S., El Albani, A., Chellai, E.H., 2006. Facies distribution of Lower–Cambrian cryptic microbial and epibenthic archaeocyathan-microbial communities in the western Anti-Atlas, Morocco. Sedimentology 53, 35–53.
Álvaro, J.J., Zamora, S., Clausen, S., Vizcaïno, D., Smith, A.B., 2013a. The role of abiotic factors in the Cambrian Substrate Revolution: a review from the benthic community replacements of West Gondwana. Earth-Science Reviews 118, 69–82.

Álvaro, J.J., Ahlberg, P., Babcock, L.E., Bordonaro, O.L., Choi, D.K., Cooper, R.A., Ergaliev, G.K., Gapp, I.W., Ghobadi Pour, M., Hughes, N.C., Jago, J.B., Koronikov, I., Laurie, J.R., Lieberman, B.S., Paterson, J.R., Pegel, T.V., Popov, L.E., Rushton, A.W. A., Sukhov, S.S., Tortello, M.F., Zhou, Z., Żylińska, A., 2013b. Global Cambrian trilobite palaeobiogeography assessed using parsimony analysis of endemicity. In: Harper, D.A.T., Servais, T. (Eds.), Early Palaeozoic Biogeography and Palaeogeography, Geological Society Memoir, vol. 38, pp. 269–292.
Álvaro, J.J., Shields, G.A., Ahlberg, P., Jensen, S., Palacios, T., 2016. Ediacaran–Cambrian phosphorites from the western margins of Gondwana and Baltica. Sedimentology 63, 350–377.
Álvaro, J.J., Ghobadi Pour, M., Sánchez-García, T., Kebria-ee Zadeh, M.R., Hairapetian, V., Popov, L.E., 2022. Stratigraphic and volcanic signatures of Miaolingian–late Ordovician rift pulses in the Alborz Mountains, northern Iran. Journal of Asian Earth Sciences 233, 105240.
Álvaro, J.J., Sánchez-García, T., Casas, J.M., 2024. The Cambrian Atlas–Ossa-Morena–North Armorican Rift, West Gondwana: along- and off-axis stratigraphic and volcano-tectonic patterns. In: Nance, R.D., Strachan, R.A., Quesada, C., Lin, S. (Eds.), Supercontinents, Orogenesis and Magmatism, Geological Society, London, Special Publications, vol. 542, pp. 465–505.
Balthasar, U., Cusack, M., 2015. Aragonite-calcite seas – quantifying the gray area. Geology 43, 99–102.
Bayet-Goll, A., Chen, J., Moussavi-Harami, R., Mahboubi, A., 2015. Depositional processes of ribbon carbonates in Middle Cambrian of Iran (Deh-Sufiyan Formation, Central Alborz). Facies 61, 9.
Bayet-Goll, A., Geyer, G., Daraei, M., 2018. Tectonic and eustatic controls on the spatial distribution and stratigraphic architecture of late early Cambrian successions at the northern Gondwana margin: the siliciclastic-carbonate successions of the Lalun Formation in central Iran. Marine and Petroleum Geology 98, 199–228.
Bayet-Goll, A., Daraei, M., Geyer, G., Bahrami, N., Bagheri, F., 2021. Environmental constraints on the distribution of matground and mixground ecosystems across the Cambrian Series 2–Miaolingian boundary interval in Iran: a case study from the central sector of northern Gondwana. Journal of African Earth Sciences 176, 104120.
Bayet-Goll, A., Daraei, M., Geyer, G., Carvalho, C., Bahrami, N., 2023. Exotic facies episodes of a carbonate platform: implications for middle and late Cambrian ecosystems and impact of bioturbation in the Alborz Basin, Iran. In: Cónsole-Gonella, C., de Valais, S., Díaz-Martínez, I., Citton, P., Verde, M. (Eds.), Ichnology in Shallow-marine and Transitional Environments, Geological Society, London, Special Publication, vol. 522, pp. 141–174.
Bednarick, A.L., Bucholz, C.E., DePaolo, D.J., Stolper, D.A., 2024. Temporal covariation of island arc and Sr isotopes and seawater chemistry over the past 2 billion years. Proceedings of the National Academy of Sciences of the United States of America 121 (43), e2401832121.
Beny-Bassez, C., Rouzaud, J.N., 1985. Characterization of carbonaceous materials by correlated electron and optical microscopy and Raman microspectroscopy. Scanning Electron Microscopy 1, 119–132.
Berg-Madsen, V., 1986. Middle Cambrian cystoid (*sensu lato*) stem columnals from Bornholm, Denmark. Lethaia 19, 67–80.
Berner, R.A., 2006. GEOCARBSULF: a combined model for Phanerozoic atmospheric $O_2$ and $CO_2$. Geochimica et Cosmochimica Acta 70, 5653–5664.
Berner, R.A., 2009. Phanerozoic atmospheric oxygen: new results using the GEOCARBSULF model. American Journal of Science 309, 603–606.
Betzler, C., Lindhorst, S., Reijmer, J.J.G., Braga, J.C., Lüdmann, T., Bialik, O.M., Reolid, J., Geßner, A.L., Hainbucher, D., Bissesur, D., 2023. Carbonate platform drowning caught in the act: the sedimentology of Saya de Malha Bank (Indian Ocean). Sedimentology 70, 78–99.
Beyssac, O., Rouzaud, J.N., Goffe, B., Brunet, F., Chopin, C., 2002. Graphitization in a high-pressure, low-temperature metamorphic gradient: a Raman microspectroscopy and HRTEM study. Contributions to Mineralogy and Petrology 143, 19–31.
Botting, J.P., Muir, L.A., 2018. Early sponge evolution: a review and phylogenetic framework. Palaeoworld 27, 1–29.
Bower, D.M., Steele, A., Fries, M.D., Kater, L., 2013. Micro Raman spectroscopy of carbonaceous material in microfossils and meteorites: improving a method for life detection. Astrobiology 13, 103–113.
Brandano, M., Lustrino, M., Cornacchia, I., Sprovieri, M., 2015. Global and regional factors responsible for the drowning of the Central Apennine Chattian carbonate platforms. Geological Journal 50, 575–591.
Brett, C.E., Liddell, W.D., Derstler, K.L., 1983. Late Cambrian hard substrate communities from Montana/Wyoming: the oldest known hardground encrusters. Lethaia 16, 281–289.
Brett, C.E., Allison, P.A., DeSantis, M., Liddell, W.D., Kramer, T., 2009. Sequence stratigraphy, cyclic facies, and lagerstätten in the Middle Cambrian Wheeler and Marjum Formations, Great Basin, Utah. Palaeogeography Palaeoclimatology Palaeoecology 277, 9–33.
Brunton, F.R., Dixon, O.A., 1994. Siliceous sponge-microbe biotic associations and their recurrence through the Phanerozoic as reef mound constructors. Palaios 9, 370–387.
Buatois, L., Mángano, M.G., 2011. Ichnology. Organism-Substrate Interactions in Space and Time. Cambridge University Press, Cambridge.
Carrera, M.G., Botting, J.P., 2008. Evolutionary history of Cambrian spiculate sponges: implications for the Cambrian evolutionary fauna. Palaios 2, 124–138.
Chen, J., Chough, S.K., Han, Z., Lee, J.H., 2011. An extensive erosion surface of a strongly deformed limestone bed in the Gushan and Chaomidian formations (late Middle Cambrian to Furongian), Shandong Province, China: sequence-stratigraphic implications. Sedimentary Geology 233, 129–149.
Chen, J., Lee, J.H., Woo, J., 2014. Formative mechanisms, depositional processes, and geological implications of Furongian (late Cambrian) reefs in the North China Platform. Palaeogeography, Palaeoclimatology, Palaeoecology 414, 246–259.
Chen, X., Zhou, Y., Shields, G.A., 2022. Progress towards and improved Precambrian seawater $^{87}Sr/^{86}Sr$ curve. Earth-Science Reviews 224, 103869.
Chow, N., James, N.P., 1992. Synsedimentary diagenesis of Cambrian peritidal carbonates: evidence from hardgrounds and surface paleokarst in the Port au Port Group, Western Newfoundland. Bulletin of Canadian Petroleum Geology 40, 115–127.
Collins, L.B., Jahnert, R.J., 2014. Stromatolite research in the Shark Bay World Heritage Area. Journal of the Royal Society of Western Australia 97, 189–219.
Cordie, D.R., 2023. Analysis of the environmental impacts affecting Cambrian reef building and carbonate settings during the Miaolingian and Furongian epochs: a hypothesis for consideration. Evolving Earth 1, 100004.
Cordie, D.R., Dornbos, Q.D., 2019. Restricted morphospace occupancy of early Cambrian reef-building archaeocyaths. Paleobiology 45, 331–346.
Cowan, C.A., James, N.P., 1993. The interactions of sea-level change, terrigenous-sediment influx, and carbonate productivity as controls on the Upper Cambrian grand cycles of western Newfoundland, Canada. Geological Society of America Bulletin 105, 1576–1590.
Daraei, M., Bayet-Goll, A., Geyer, G., Bahrami, N., 2023. Late Cambrian climate change recorded by a shift from an arid carbonate platform to a storm-dominated cool-water platform at the Gondwana margin (Alborz Zone, Iran). Geological Journal 58, 795–824.
Dattilo, B.F., Hlohowskyj, S., Ripperdan, R.L., Miller, J.F., Shapiro, R.S., 2004. Stratigraphic setting of an Upper Cambrian metazoan reef between the Nopah Formation to Goodwin Formation transition in southern Nevada. In: Geological Society of America, Abstracts With Programs, vol. 36, p. 368.
Debrenne, F., 1991. Extinction of the Archaeocyatha. Historical Biology 5, 95–106.
Debrenne, F., Kruse, P.D., 1989. Cambrian Antarctic archaeocyaths. In: Crame, J.A. (Ed.), Origins and Evolution of the Antarctic Biota, Geological Society, London, Special Publication, vol. 47, pp. 15–28.
Debrenne, F., Reitner, J., 2001. Sponges, cnidarians, and ctenophores. In: Zhuravlev, A. Yu., Riding, R. (Eds.), The Ecology of the Cambrian Radiation. Columbia University Press, New York, pp. 301–325.
Debrenne, F., Rozanov, A.Yu., Webers, G.F., 1984. Upper Cambrian Archaeocyatha from Antarctica. Geological Magazine 121, 291–299.
Debrenne, F., Zhuravlev, A.Yu., Kruse, P.D., 2015. Systematic descriptions: Archaeocyatha. In: Treatise on Invertebrate Paleontology, Part E (Revised), Porifera, Volumes 4–5 (Hypercalcified Porifera). The University of Kansas, Paleontological Institute, Lawrence KS, pp. 923–1084.
Devaere, L., Korn, D., Ghaderi, A., Struck, U., Bavandpur, A.K., 2021. New and revised small shelly fossil record from the lower Cambrian of northern Iran. Papers in Palaeontology 7, 2141–2181.
Droser, M.L., Li, X., 2001. The Cambrian radiation and the diversification of sedimentary fabrics. In: Zhuravlev, A.Yu., Riding, R. (Eds.), The Ecology of the Cambrian Radiation. Columbia University Press, New York, pp. 137–169.
Dzik, J., 1994. Evolution of "small shelly fossils" assemblages of the Early Paleozoic. Acta Palaeontologica Polonica 39, 247–313.
Erdtmann, B., Henningsmoen, G., Welsch, M., Windolph, M.L., 1984. Fossiler frå Digermulhalvøya. Ottar 146, 10–30.
Finks, R.M., 2003a. Paleozoic Demospongea: morphology and phylogeny. In: Kaesler, R. L. (Ed.), Treatise on Invertebrate Paleontology, Part E, Porifera (Revised), vol. 2. Geological Society of America and University of Kansas, Boulder, Colorado and Lawrence, Kansas, pp. 63–80.
Finks, R.M., 2003b. Evolution and ecologic history during Paleozoic times. In: Kaesler, R. L. (Ed.), Treatise on Invertebrate Paleontology, Part E, Porifera (Revised), vol. 2. Geological Society of America and University of Kansas, Boulder, Colorado and Lawrence, Kansas, pp. 261–274.
Geyer, G., Bayet-Goll, A., Wilmsen, M., Mahboubi, A., Moussavi-Harami, R., 2014. Lithostratigraphic revision of the middle Cambrian (Series 3) and upper Cambrian (Furongian) in northern and central Iran. Newsletters on Stratigraphy 47, 21–59.
Ghobadi Pour, M., Popov, L.E., Álvaro, J.J., Amini, A., Hairapetian, V., Jahangir, H., 2022. Ordovician of North Iran: new lithostratigraphy, palaeogeography and biogeographical links with South China and the Mediterranean peri-Gondwana margin. Bulletin of Geosciences 97, 465–538.
Gill, B.C., Lyons, T.W., Young, S.A., Kump, L.R., Knoll, A.H., Saltzman, M.R., 2011. Geochemical evidence for widespread euxinia in the later Cambrian ocean. Nature 469, 80–83.
Glass, L.M., Phillips, D., 2006. The Kalkanrindji continental flood basalt province: a new Cambrian large igneous province in Australia with possible links to faunal extinctions. Geology 34, 461–464.
Gómez, F.J., Astini, R.A., 2015. Sedimentology and sequence stratigraphy from a mixed (carbonate-siliciclastic) rift to passive margin transition: the Early to Middle Cambrian of the Argentine Precordillera. Sedimentary Geology 316, 39–61.
Guensburg, T.E., Rozhnov, S.V., 2014. A unique edrioasteroid from the Upper Middle Cambrian of Iran, its phylogenetic implications and paleoecology. Paleontological Journal 48, 401–406.
Hamdi, B., 1995. Precambrian–Cambrian deposits in Iran. In: Treatise on the Geology of Iran, vol. 20. Geological Survey of Iran, Tehran, pp. 1–353 (in Farsi).
Hamdi, B., Rozanov, A.Y., Zhuravlev, A.Yu., 1995. Latest middle Cambrian metazoan reef from northern Iran. Geological Magazine 132, 367–373.
Han, Z., Zhang, X., Chi, N., Han, M., Woo, J., Lee, H.S., Chen, J., 2015. Cambrian oncoids and other microbial-related grains on the North China Platform. Carbonates and Evaporites 30, 373–386.

Hicks, M., 2006. A new genus of early Cambrian coral in Esmeralda County, Southwestern Nevada. Journal of Paleontology 80, 609–615.
Holmer, L.E., Kebria-ee Zadeh, M.R., Popov, L.E., Ghobadi Pour, M., Álvaro, J.J., Hairapetian, V., Zhang, Z., Cherns, L., 2019. Cambrian rhynchonelliform nisusioid brachiopods: phylogeny and distribution. Papers in Palaeontology 5, 559–575.
Hong, J., Cho, S.H., Choh, S.J., Woo, J., Lee, D.J., 2012. Middle Cambrian siliceous sponge-calcimicrobe buildups (Daegi Formation, Korea): metazoan buildup constituents in the aftermath of the early Cambrian extinction event. Sedimentary Geology 253–254, 47–57.
Hong, J., Choh, S.J., Lee, D.J., 2015. Untangling intricate microbial-sponge frameworks: the contributions of sponges to Early Ordovician reefs. Sedimentary Geology 318, 75–84.
Hong, J., Lee, J.H., Choh, S.J., Lee, D.J., 2016. Cambrian series 3 carbonate platform of Korea dominated by microbial-sponge reefs. Sedimentary Geology 341, 58–69.
Hong, J., Park, J., Kim, D., Cho, E., Kim, S.M., 2022. Relatively deep subtidal microbial-lithistid sponge reef communities in Lower Ordovician rocks reveal incipient escalation of the Great Ordovician Biodiversification Event. SSRN. https://doi.org/10.2139/ssrn.4067369.
Horton, B.K., Hassanzadeh, J., Stockli, D.F., Axen, G.J., Gillis, R.J., Guest, B., Amini, A., Fakhari, M.D., Zamanzadeh, S.M., Grove, M., 2008. Detrital zircon provenance of Neoproterozoic to Cenozoic deposits in Iran: implications for chronostratigraphy and collisional tectonics. Tectonophysics 451, 97–122.
Hough, M.L., Shields, G.A., Evins, L.Z., Strauss, H., Henderson, R.A., McKenzie, S., 2006. A major sulphur isotope event at c. 510 Ma: a possible anoxia-extinction-volcanism connection during the Early–Middle Cambrian transition? Terra Nova 18, 257–263.
Jahangir, H., Ghobadi Pour, M., Ashuri, A., Amini, A., 2016. Terminal Cambrian and Early Ordovician (Tremadocian) conodonts from Eastern Alborz, north-central Iran. Alcheringa 40, 219–243.
James, N.P., Gravestock, D.I., 1990. Lower Cambrian shelf and shelf margin buildups, Flinders Ranges, South Australia. Sedimentology 37, 455–480.
Johns, R.A., Dattilo, B.F., Spincer, B., 2007. Neotype and redescription of the Upper Cambrian anthaspidellid sponge *Wilbernicyathus donegani* Wilson, 1950. Journal of Paleontology 81, 435–444.
Kidwell, S.M., Jablonski, D., 1983. Taphonomic feedback. Geological consequences of shell accumulation. In: Tevesz, M.J.S., McCall, P.L. (Eds.), Biotic Interactions in Recent and Fossil Benthic Communities. Plenum Press, New York, pp. 195–248.
Kiessling, W., Simpson, C., 2011. On the potential for ocean acidification to be a general cause of ancient reef crises. Global Change Biology 17, 56–67.
Phanerozoic reef patterns. In: Kiessling, W., Flugel, E., Golonka, J. (Eds.), 2002. Society for Sedimentary Geology (SEPM), Special Publication 72 (775 pp).
Kruse, P.D., 1991. Cyanobacterial-archaeocyathan-radiocyathan bioherms in the Wirrealpa Limestone of South Australia. Canadian Journal of Earth Sciences 28, 601–615.
Kruse, P.D., 1996. Update on the northern Australian Cambrian sponges *Rankenella*, *Jawonya* and *Wagima*. Alcheringa 20, 161–178.
Kruse, P.D., Reitner, J.R., 2014. Northern Australian microbial-metazoan reefs after the mid–Cambrian mass extinction. Memoirs of the Association of Australasian Palaeontologists 1, 31–53.
Kruse, P., Zhuravlev, A., 2008. Middle–late Cambrian *Rankenella-Girvanella* reefs of the Mila Formation, northern Iran. Canadian Journal of Earth Sciences 45, 619–639.
Kruse, P.D., Zhuravlev, A., James, N., 1995. Primordial metazoan-calcimicrobial reefs: Tommotian (Early Cambrian) of the Siberian Platform. Palaios 10, 291–321.
Kruse, P.D., Gandin, A., Debrenne, F., Wood, R., 1996. Early Cambrian bioconstructions in Zavkhan Basin of western Mongolia. Geological Magazine 133, 429–444.
Kushan, B., 1973. Stratigraphie und Trilobiten fauna in der Mila-Formation (Mittelkambrium–Tremadoc) im Alborz-Gebirge (N-Iran). Palaeontographica Abteilung A 144, 113–165.
Kushan, B., 1978. Stratigraphy and trilobite fauna of the Mila Formation (Middle Cambrian–Tremadocian) of the Alborz Range, North Iran. In: Geological Survey of Iran, Report 49, pp. 1–70.
Lahfid, A., Beyssac, O., Deville, E., Negro, F., Chopin, C., Goffé, B., 2010. Evolution of the Raman spectrum of carbonaceous material in low-grade metasediments of the Glarus Alps (Switzerland). Terra Nova 22, 354–360.
Lasemi, Y., Amin-Rasouli, H., 2007. Archaeocyathan buildups within an entirely siliciclastic succession: new discovery in the Toyonian Lalun Formation of northern Iran, the Proto-Paleotethys passive margin of northern Gondwana. Sedimentary Geology 201, 302–320.
Lasemi, Y., Amin-Rasouli, H., 2016. The lower–middle Cambrian transition and the Sauk I–II unconformable boundary in Iran, a record of late early Cambrian global Hawke Bay regression. In: Sorkhabi, R. (Ed.), Tectonic, Evolution, Collision, and Seismicity of Southwest Asia: In Honor of Manuel Berberian's Forty-five Years of Research Contributions, Geological Society of America, Special Paper, vol. 525, pp. 343–366.
Lee, J.H., 2024. Limiting the known range of archaeocyath to the middle Cambrian: *Antarcticocyathus webersi* Debrenne et al. 1984 is a lithistid sponge. Historical Biology 36, 209–213.
Lee, J.H., Riding, R., 2018. Marine oxygenation, lithistid sponges, and the early history of Paleozoic skeletal reefs. Earth-Science Reviews 181, 98–121.
Lee, J.H., Chen, J., Chough, S.K., 2010. Paleoenvironmental implications of an extensive maceriate microbialite bed in the Furongian Chaomidian Formation, Shandong Province, China. Palaeogeography, Palaeoclimatology, Palaeoecology 297, 621–632.
Lee, J.H., Chen, J., Choh, S.J., Lee, D.J., Han, Z., Chough, S.W., 2014. Furongian (Late Cambrian) sponge-microbial maze-like reefs in the North China Platform. Palaios 29, 27–37.
Lee, J.H., Chen, J., Woo, J., 2015a. The earliest Phanerozoic carbonate hardground (Cambrian Stage 5, Series 3): implications to the paleoseawater chemistry and early adaptation of hardground fauna. Palaeogeography, Palaeoclimatology, Palaeoecology 440, 172–179.
Lee, J.H., Chen, J., Chough, S.K., 2015b. The middle–late Cambrian reef transition and related geological events: a review and new view. Earth-Science Reviews 145, 66–84.
Lee, J.H., Hong, J., Choh, S.J., Lee, D.J., Woo, J., Riding, R., 2016a. Early recovery of sponge framework reefs after Cambrian archaeocyath extinction: Zhangxia Formation (early Cambrian Series 3), Shandong, North China. Palaeogeography, Palaeoclimatology, Palaeoecology 457, 269–276.
Lee, J.H., Woo, J., Lee, D.J., 2016b. The earliest reef-building anthaspidellid sponge *Rankenella zhangxianensis* n. sp. from the Zhangxia Formation (Cambrian Series 3), Shandong Province, China. Journal of Paleontology 90, 1–9.
Lee, J.H., Dattilo, B.F., Mrozek, S., Miller, J.F., Riding, R., 2019. Lithistid sponge-microbial reefs, Nevada, USA: filling the late Cambrian 'reef gap'. Palaeogeography, Palaeoclimatology, Palaeoecology 520, 251–262.
Lee, J.H., Cho, S.H., Jung, D.Y., Choh, S.J., Lee, D.J., 2021. Ribbon rocks revisited: the upper Cambrian (Furongian) Hwajeol Formation, Taebaek Group, Korea. Facies 67, 1–19.
Leys, S.P., Yahel, G., Reidenbach, M.A., Tunnicliffe, V., Shavit, U., Reiswig, H.M., 2011. The sponge pump: the role of current induced flow in the design of the sponge body plan. PLoS One 6 (12), e27787.
Li, Q., Li, Y., Wang, J., Kiessling, W., 2015. Early Ordovician lithistid sponge-*Calathium* reefs of the Yangtze Platform and their paleoceanographic implications. Palaeogeography, Palaeoclimatology, Palaeoecology 425, 84–96.
Li, H., Li, F., Li, X., Zeng, K., Gong, Q., Yi, C., Wang, Z., 2021. Development and collapse of the early Cambrian shallow-water carbonate factories in the Hannan-Micangshan area, South China. Palaeogeography, Palaeoclimatology, Palaeoecology 583, 110665.
Li, Y.F., Li, F., Webb, G.E., Chen, J., 2024. Intense intrusion of low-oxygen waters in mid–Cambrian surface ocean carbonate factories. Chemical Geology 669, 122360.
Loi, A., Pillola, L., Leone, F., 1995. The Cambrian and Early Ordovician of south-western Sardinia. Rendiconti del Seminario della Facoltà di Scienze dell'Università di Cagliari 65, 63–71 supplement volume.
Ludeman, D.A., Reidenbach, M., Leys, S., 2017. The energetic cost of filtrators by demosponges and their behavioural response to ambient currents. Journal of Experimental Biology 220, 995–1007.
Luo, C., Schäfer, N., Duda, J.P., Li, L.X., 2014. Preservation of organic matter in sponge fossils: a case study of 'round sponge fossils' from the Cambrian Chengjiang Biota with Raman spectroscopy. Göttingen Contributions to Geosciences 77, 29–38.
Maldonado, M., Aguilar, R., Blanco, J., Garcia, S., Serrano, A., Punzon, A., 2015. Aggregated clumps of lithistid sponges: a singular, reef-like bathyal habitat with relevant paleontological connections. PLoS One 10, e0125378.
Marshall, C.P., Edwards, H.G.M., Jehlicka, J., 2010. Understanding the application of Raman spectroscopy to the detection of traces of life. Astrobiology 10, 229–243.
Masse, J.P., Fenerci-Masse, M., 2013. Drowning events, development and demise of carbonate platforms and controlling factors: the Late Barremian–Early Aptian record of Southeast France. Sedimentary Geology 298, 28–52.
McKenzie, N.R., Hughes, N.C., Gill, B.C., Myrow, P.M., 2014. Plate tectonic influences on Neoproterozoic–early Paleozoic climate and animal evolution. Geology 42, 127–130.
Mitchell, R.N., Evans, D.A.D., Kilian, T.M., 2010. Rapid Early Cambrian rotation of Gondwana. Geology 38, 755–758.
Morrow, C., Cárdenas, P., 2015. Proposal for a revised classification of the Demospongiae (Porifera). Frontiers in Zoology 12, 7.
Mrozek, S., Dattilo, B.F., Hicks, M., Miller, J.F., 2003. Metazoan reefs from the Upper Cambrian of the Arrow Canyon Range, Clark County, Nevada. In: Geological Society of America, Abstracts With Programs, vol. 35, p. 500.
Myrow, P.M., Goodge, J.W., Brock, G.A., Betts, M.J., Park, T.S., Hughes, N.C., Gaines, R. R., 2024. Tectonic trigger to the first major extinction of the Phanerozoic: the early Cambrian Sinsk event. Science Advances 10, eadl3452.
Neilson, J.E., Brasier, A.T., North, C.P., 2016. Primary aragonite and high-Mg calcite in the late Cambrian (Furongian). Potential evidence from marine carbonates in Oman. Terra Nova 28, 306–315.
Nielsen, A.T., Schovsbo, N.H., 2015. The regressive early–mid Cambrian "Hawke Bay event" in Baltoscandia: epeirogenic uplift in concert with eustasy. Earth-Science Reviews 151, 288–350.
Noffke, N., Gerdes, G., Klenke, T., Krumbein, W.E., 2001. Microbially induced sedimentary structures indicating climatological, hydrological and depositional conditions within Recent and Pleistocene coastal facies zones (southern Tunisia). Facies 44, 23–30.
Noffke, N., Beraldi-Campesi, H., Callefo, F., Carmona, N., Cuadrado, D.G., Hickman-Lewis, K., Homann, M., Mitchell, R., Sheldon, N., Westall, F., Xiao, S., 2022. Treatise Online No. 162: Part B, Volume 2, Chapter 5: Microbially Induced Sedimentary Structures (MISS). Treatise Online. https://doi.org/10.17161/to.vi.18111.
Oslager, D.A., Montañez, I.P., 1996. Cross-platform architecture of a sequence boundary in mixed siliciclastic-carbonate lithofacies, Middle Cambrian, southern Great Basin, USA. Sedimentology 43, 197–217.
Ou, Z., Liu, J., Meng, F., 2025. Evaluating baseline correction in Raman Spectroscopy: a novel cross-wavelength correlation approach for low-maturity organic matter. Journal of Raman Spectroscopy. https://doi.org/10.1002/jrs.6825.
Palmer, A.R., James, N.P., 1980. The Hawke Bay event: a circum-Iapetus regression near the Lower–Middle Cambrian boundary. In: Wones, D.R. (Ed.), The Caledonides in the USA, Department of Geological Sciences, Virginia Polytechnic Institute and State University, Memoir, vol. 2, pp. 15–18.
Papineau, D., 2010. Global biogeochemical changes at both ends of the Proterozoic: insights from phosphorites. Astrobiology 10, 165–181.

Park, T.Y., Woo, J., Lee, D.J., Lee, D.C., Lee, S.B., Han, Z., Chough, S.K., Choi, D.K., 2011. A stem-group cnidarian described from the mid–Cambrian of China and its significance for cnidarian evolution. Nature Communications 2, 442.
Park, T.Y., Kihm, J.H., Woo, J., Zhen, Y.Y., Engelbretsen, M., Hong, J., Choh, S.J., Lee, D. J., 2016. Cambrian stem-group cnidarians with a new species from the Cambrian Series 3 of the Taebaeksan Basin, Korea. Acta Geologica Sinica 90, 827–837.
Peel, J., 2017. The oldest pelmatozoan encrusted hardground and holdfasts from Laurentia (Cambrian Series 2–3). GFF 139, 195–204.
Peng, S.C., Geyer, G., Hamdi, B., 1999. Trilobites from the Shahmirzad section, Alborz Mountains, Iran: their taxonomy, biostratigraphy and bearing for international correlation. Beringeria 24, 3–64.
Perejón, A., Moreno-Eiris, E., 2003. Arqueociatos del Bilbiliense (Cámbrico inferior) del manto del Esla, Cordillera Cantábrica, Norte de España. Boletín de la Real Sociedad Española de Historia Natural (Sección Geológica) 98, 51–71.
Peters, S.E., Gaines, R.R., 2012. Formation of the 'Great Unconformity' as a trigger for the Cambrian explosion. Nature 484, 363–366.
Popov, L.E., Ghobadi Pour, M., Hosseini, M., Holmer, L.E., 2009. Furongian linguliform brachiopods from the Alborz Mountains, Iran. Memoirs of the Association of Australasian Palaeontologists 37, 103–122.
Popov, L.E., Ghobadi Pour, M., Kebria-ee Zadeh, M.R., Shahbeik, S., 2011. First record of silicified Cambrian (Furongian) rhynchonelliform brachiopods from the Mila Formation, Alborz Range, Iran. Memoirs of the Association of Australasian Palaeontologists 42, 193–207.
Popov, L.E., Kebria-ee Zadeh, M.R., Ghobadi Pour, M., Holmer, L., Modzalevskaya, T.L., 2013. Cambrian (Furongian) rhynchonelliform brachiopods from the eastern Alborz Mountains, Iran. Bulletin of Geosciences 88, 525–538.
Pratt, B.R., Spincer, B.R., Wood, R.A., Zhuravlev, A.Yu., 2001. Ecology and evolution of Cambrian reefs. In: Zhuravlev, A.Yu., Riding, R. (Eds.), The Ecology of the Cambrian Radiation. Columbia University Press, New York, pp. 254–274.
Pruss, S.B., Karbowski, G., Zhuravlev, A.Yu., Webster, M., Smith, E.F., 2024. Dead clade walking: the persistence of *Archaeocyathus* in the aftermath of early Cambrian reef extinction in the western United States. Palaios 39, 210–224.
Quirico, E., Montagnac, G., Rouzaud, J.N., Bonal, L., Bourot Denise, M., Duber, S., Reynard, B., 2009. Precursor and metamorphic condition effects on Raman spectra of poorly ordered carbonaceous matter in chondrites and coals. Earth and Planetary Science Letters 287, 185–193.
Raja, N.B., Pandolfi, J.M., Kiessling, W., 2023. Modularity explains large-scale reef booms in Earth's history. Facies 69, 15.
Rankey, E.C., Walker, K.R., Srinivasan, K., 1994. Gradual establishment of Iapetan "passive" margin sedimentation: stratigraphic consequences of Cambrian episodic tectonism and eustasy, southern Appalachians. Journal of Sedimentary Research B64, 298–310.
Reitner, J., Mehl, D., 1995. Early Paleozoic diversification of sponges: new data and evidence. Geologische Paläontologische Mitteilungen Universität Innsbruck 20, 335–347.
Riding, R., 2002. Structure and composition or organic reefs and carbonate mud mounds: concepts and categories. Earth-Science Reviews 58, 163–231.
Riding, R., Liang, L., 2005. Geobiology of microbial carbonates: metazoan and seawater saturation state influences on secular trends during the Phanerozoic. Palaeogeography, Palaeoclimatology, Palaeoecology 219, 101–115.
Riding, R., Zhuravlev, A.Yu., 1995. Structure and diversity of oldest sponge-microbe reefs: Lower Cambrian, Aldan River, Siberia. Geology 23, 649–652.
Rothman, D.H., 2002. Atmospheric carbon dioxide levels for the last 500 million years. Proceedings of the National Academy of Sciences of the United States of America 99, 4167–4171.
Rowland, S.M., Shapiro, R.S., 2002. Reef patterns and environmental influences in the Cambrian and earliest Ordovician. In: Kiessling, W., Flügel, E., Golonka, J. (Eds.), Phanerozoic Reef Patterns, SEPM Society for Sedimentary Geology, vol. 72, pp. 95–128.
Rozhnov, S., 2001. Evolution of the hardground community. In: Zhuravlev, A.Yu., Riding, R. (Eds.), The Ecology of the Cambrian Radiation. Columbia University Press, New York, pp. 238–253.
Rozhnov, S., 2015. Unusual eocrinoid (?) stem and columnals from the Late Cambrian of Northern Iran. In: The Rise of Animal Life – Promoting Geological Heritage: Challenges and Issues, Marrakesh 05-10th October 2015, Abstracts, pp. 116–117.
Rozhnov, S.V., Parsley, R., 2017. A new cornute (Homalozoa: Echinodermata) from the uppermost Middle Cambrian (stage 3, Furongian) from Northern Iran: its systematics and functional morphology. Paleontological Journal 51, 500–509.
Ruttner, A., Nabavi, M., Hajian, J., 1968. Geology of the Shirgesht area (Tabas area, east Iran). In: Geological Survey of Iran, Reports, vol. 4, pp. 1–133.
Saltzman, M.R., Young, S.A., Kump, L.R., Gill, B.C., Lyons, T.W., Runnegar, B., 2011. Pulse of atmospheric oxygen during the late Cambrian. Proceedings of the National Academy of Sciences of the United States of America 108, 3876–3881.
Saltzman, M.R., Edwards, C.T., Adrain, J.M., Westrop, S.R., 2015. Persistent oceanic anoxia and elevated extinction rates separate the Cambrian and Ordovician radiations. Geology 43, 807–810.
Sandberg, P., 1983. An oscillating trend in Phanerozoic non-skeletal carbonate mineralogy. Nature 305, 19–22.
Schito, A., Spina, A., Corrado, S., Cirilli, S., Romano, C., 2019. Comparing optical and Raman spectroscopic investigations of phytoclasts and sporomorphs for thermal maturity assessment: the case study of Hettangian continental facies in the Holy Cross Mts. (central Poland). Marine and Petroleum Geology 104, 331–345.
Schito, A., Ataoubat, A., Muirhead, D.K., Calcagni, R., Galimberti, R., Romano, C., Spina, A., Corrado, S., 2022. An insight on the polyphase thermal history of the Internal Rif (Northern Morocco) through Raman micro-spectroscopy. Italian Journal of Geosciences 141, 104–119.
Schuster, A., Erpenbeck, D., Pisera, A., Hooper, J., Bryce, M., Fromont, J., Wörheide, G., 2015. Deceptive desmas: molecular phylogenetics suggests a new classification and uncovers convergent evolution of lithistid demosponges. PLoS One 10, e116038.
Scotese, C.R., Barret, S.F., 1990. Gondwana's movement over the South Pole during the Palaeozoic: evidence from lithological indicators of climate. In: McKerrow, W.S., Scotese, C.R. (Eds.), Palaeozoic Palaeogeography and Biogeography, Geological Society Memoirs, vol. 12, pp. 75–85.
Scrutton, C.T., 1997. The Palaeozoic corals, I: origins and relationships. Proceedings of the Yorkshire Geological Society 51, 177–208.
Seilacher, A., 2007. Trace Fossil Analysis. Springer Verlag, Berlin (226 pp.).
Seilacher, A., MacClintock, C., 2005. Crinoid anchoring strategies for soft-bottom dwelling. Palaios 20, 224–240.
Shapiro, R.S., Awramik, S.M., 2006. *Favosamaceria cooperi* New group and form: a widely dispersed, time-restricted thrombolite. Journal of Paleontology 80, 411–422.
Shapiro, R.S., Rigby, J.K., 2004. First occurrence of an *in situ* anthaspidellid sponge in a dendrolite mound (upper Cambrian; Great Basin, USA). Journal of Paleontology 78, 645–650.
Signor, P.W., 1992. Taxonomic diversity and faunal turnover in the Early Cambrian: did the most severe mass extinction of the Phanerozoic occur in the Botomian stage?. In: The Paleontological Society, Special Publications, vol. 6, p. 272.
Smith, B.P., Cantine, M.D., Bergmann, K.D., Ramos, E.J., Martindale, R.C., Kerans, C., 2021. Arid coastal carbonates and the Phanerozoic record of carbonate chemistry. AGU Advances 2, e2021AV000386.
Sorci, A., Cirilli, S., Spina, A., Ghorbani, M., Rettori, R., 2023. Facies analysis and depositional environment of a late Cambrian mixed carbonate-siliciclastic ramp from the Zard Kuh Mountain (Zagros Basin, south-western Iran). Sedimentary Geology 449, 106370.
Spina, A., Cirilli, S., Ghorbani, M., Rettori, R., Sorci, A., Servais, T., 2021. Middle–late Cambrian acritarchs of the Zagros Basin, southwestern Iran. Palynology 45, 171–186.
Srinivasan, K., Walker, W.R., 1993. Sequence stratigraphy of an intrashelf basin carbonate ramp to rimmed platform transition: Maryville Limestone (Middle Cambrian), southern Appalachians. Geological Society of America Bulletin 105, 883–896.
Stanley, S.M., Hardie, L.A., 1998. Secular oscillations in the carbonate mineralogy of reef-building and sediment-producing organisms driven by tectonically forced shifts in seawater chemistry. Palaeogeography, Palaeoclimatology, Palaeoecology 144, 3–19.
Stöcklin, J., 1972. Iran central, septentrional et oriental. Lexique Stratigraphique International, Volume III (Asie). Fascicule 9 (Iran). CNRS, Paris (283 pp.).
Stöcklin, J., Ruttner, A., Nabavi, M., 1964. New data on the Lower Paleozoic and pre–Cambrian of North Iran. In: Geological Survey of Iran, Report, vol. 1, pp. 1–29.
Sumrall, C.D., Sprinkle, J., Guensburg, T.E., 1997. Systematics and paleoecology of Late Cambrian echinoderms from the Western United States. Journal of Paleontology 71, 1091–1109.
Taylor, P.D., Wilson, M.A., 2003. Palaeoecology and evolution of marine hard substrate communities. Earth-Science Reviews 62, 1–103.
Torromé, D., Aurell, M., Bádenas, B., 2022. A mud-dominated coastal plain to lagoon with emerged carbonate mudbanks: the imprint of low-amplitude sea level cycles (mid–Upper Cretaceous, South Iberian Ramp). Sedimentary Geology 436, 106178.
Van der Meer, D.G., Scotese, C.R., Mills, B.J.W., Sluijs, A., van den Berg van Saparoea, A. P., van de Weg, R.M.B., 2022. Long-term Phanerozoic global mean sea level: insights from strontium isotope variations and estimates of continental glaciation. Gondwana Research 111, 103–121.
Van der Meer, D.G., Stap, L.B., Scotese, C.R., Mills, B.J.W., Sluijs, A., van Hinsbergen, D. J.J., 2025. Phanerozoic orbital-scale glacio-eustatic variability. Earth and Planetary Science Letters 667, 119526.
Védrine, S., Strasser, A., Hug, W., 2007. Oncoid growth and distribution controlled by sea-level fluctuations and climate (Late Oxfordian, Swiss Jura Mountains). Facies 53, 535–552.
Wang, J., Tarhan, L.D., Jacobson, A.D., Oehlert, A.M., Planavsky, N.J., 2023. The evolution of the marine carbonate factory. Nature 615, 1–5.
Wang, W., Dai, W., Vayda, P., Luo, J., Liu, Y., Hua, H., Xiao, S., 2025. Fortunian archaeocyath sponges acquired biomineralization in the beginning of the Cambrian explosion. Geology 53 (6), 540–544.
Webby, B.D., 2002. Patterns of Ordovician reef development. In: Kiessling, W., Flügel, E., Golonka, J. (Eds.), Phanerozoic Reef Patterns, SEPM Special Publication, vol. 72, pp. 129–179.
Williams, A., Carlson, S.J., Manceñido, M.O., MacKinnon, D.I., Savage, N.M., Yu-Gan, J., Grant, R.E., Blodgett, R.B., Dagys, A.S., Jia-Yu, R., Brunton, C.H.C., Cooper, P., Boucot, A.J., Alvárez, F., Dong-Li, S., Owen, E.F., 2002. Part H, Brachiopoda (Revised), Volume 4. The University of Kansas, Paleontological Institute, Lawrence.
Wilson, M.A., Palmer, T.J., 1992. Hardgrounds and hardground faunas. In: University of Wales, Institute of Earth Studies Publications, vol. 9, pp. 1–131.
Wittke, H.W., 1984. Middle and Upper Cambrian trilobites from Iran: their taxonomy, stratigraphy and significance for provincialism. Palaeontolographica, Abteilung A 183, 91–161.
Wood, R., 1999. Reef Evolution. Oxford University Press, New York (426 pp.).
Wood, R., Zhuravlev, A.Yu., 2012. Escalation and ecological selectively of mineralogy in the Cambrian radiation of skeletons. Earth-Science Reviews 115, 249–261.
Wood, R.A., Evans, K.R., Zhuravlev, A.Yu., 1992. A new post–early Cambrian archaeocyath from Antarctica. Geological Magazine 129, 491–495.
Wood, R., Zhuravlev, A.Yu., Anaaz, C.T., 1993. The ecology of lower Cambrian buildups from Zuune arts, Mongolia: implications for early metazoan reef evolution. Sedimentology 40, 829–858.

Wopenka, B., Pasteris, J.D., 1993. Structural characterization of kerogens to granulite-facies graphite: applicability of Raman microprobe spectroscopy. American Mineralogist 78, 533–557.
Wrona, R., Hamdi, B., 2001. Palaeoscolecid sclerites from the Upper Cambrian Mila Formation of the Shahmirzad section, Alborz Mountains, northern Iran. Acta Geologica Polonica 51, 101–107.
Xiao, Z., Latif, K., Qin, Y., Wang, H., 2018. Calcified microorganisms bloom in Furongian of the North China Platform: evidence from microbialitic-bioherm in Qijiayu section, Hebei. Open Geosciences 10, 250–260.
Yang, A., Zhu, M., Zhuravlev, A.Yu., Yuan, K., Zhang, J., Chen, Y., 2016. Archaeocyathan zonation of the Yangtze Platform: implications for regional and global correlation of lower Cambrian stages. Geological Magazine 153, 388–409.
Zamora, S., Álvaro, J.J., Vizcaïno, D., 2009. Pelmatozoan echinoderms from the Cambrian–Ordovician transition of the Iberian Chains (NE Spain): early diversification of anchoring strategies. Swiss Journal of Geosciences 102, 43–55.
Zamora, S., Clausen, S., Álvaro, J.J., Smith, A.B., 2010. Pelmatozoan echinoderms as colonizers of carbonate firmgrounds in mid–Cambrian high energy environments. Palaios 25, 764–768.
Zhuravlev, A.Yu., Hart, M.B., 1996. Reef ecosystem recovery after the Early Cambrian extinction. In: Biotic Recovery From Mass Extinction Events. Geological Society, London, Special Publication, vol. 102, pp. 79–96.
Zhuravlev, A.Yu., Naimark, E.B., 2005. Alpha, beta, or gamma: numerical view on the early Cambrian world. Palaeogeography, Palaeoclimatology, Palaeoecology 220, 207–225.
Zhuravlev, A.Yu., Wood, R.A., 2008. Eve of biomineralization: controls on skeletal mineralogy. Geology 36, 923–926.
Zhuravlev, A.Yu., Mitchell, E.G., Bowyer, F., Wood, R., Penny, A., 2022. Increases in reef size, habitat and metacommunity complexity associated with Cambrian radiation oxygenation pulses. Nature Communications 13, 7523.
Zhuravlev, A.Yu., Wood, R.A., Bowyer, F.T., 2023. Cambrian radiation speciation events driven by sea level and redoxcline changes on the Siberian Craton. Science Advances 9, eadh2558.
Zoleikhaei, Y., Mulder, J.A., Cawood, P.A., 2021. Integrated detrital rutile and zircon provenance reveals multiple sources for Cambrian sandstones in North Gondwana. Earth-Science Reviews 213, 103462.